Cellular and Molecular Life Sciences (2023) 80:155
https://doi.org/10.1007/s00018-023-04807-7

ORIGINAL ARTICLE

Dietary intake of α-ketoglutarate ameliorates α-synuclein pathology in mouse models of Parkinson's disease

Wenlong Zhang[1,2] · Liuyan Ding[1,2] · Mengran Zhang[2,3,4] · Shaohui Zheng[2,3,4] · Runfang Ma[2,3,4] · Junwei Gong[2] · Hengxu Mao[1] · Huaxi Xu[5] · Pingyi Xu[1] · Yunlong Zhang[2,3,4]

Received: 13 January 2023 / Revised: 9 May 2023 / Accepted: 10 May 2023 / Published online: 19 May 2023

Abstract

Parkinson's disease (PD) is a progressive movement disorder characterized by dopaminergic (DA) neuron degeneration and the existence of Lewy bodies formed by misfolded α-synuclein. Emerging evidence supports the benefits of dietary interventions in PD due to their safety and practicality. Previously, dietary intake of α-ketoglutarate (AKG) was proved to extend the lifespan of various species and protect mice from frailty. However, the mechanism of dietary AKG's effects in PD remains undetermined. In the present study, we report that an AKG-based diet significantly ameliorated α-synuclein pathology, and rescued DA neuron degeneration and impaired DA synapses in adeno-associated virus (AAV)-loaded human α-synuclein mice and transgenic A53T α-synuclein (A53T α-Syn) mice. Moreover, AKG diet increased nigral docosahexaenoic acid (DHA) levels and DHA supplementation reproduced the anti-α-synuclein effects in the PD mouse model. Our study reveals that AKG and DHA induced microglia to phagocytose and degrade α-synuclein via promoting C1q and suppressed pro-inflammatory reactions. Furthermore, results indicate that modulating gut polyunsaturated fatty acid metabolism and microbiota *Lachnospiraceae_NK4A136_group* in the gut-brain axis may underlie AKG's benefits in treating α-synucleinopathy in mice. Together, our findings propose that dietary intake of AKG is a feasible and promising therapeutic approach for PD.

Keywords Parkinson's disease · AKG · DHA · α-synuclein · DA neuron degeneration · Gut-brain axis

Introduction

Parkinson's disease (PD) is a common progressive neurodegenerative disorder with clinical features such as bradykinesia, rest tremor, muscular rigidity, and postural and gait dysfunction [1]. The critical pathological hallmarks of PD consist of progressive dopaminergic (DA) neuron degeneration in the substantia nigra pars compacta (SNpc) and the formation of Lewy bodies, which include misfolded α-synuclein [2]. Although dopamine-based therapies remain the gold standard pharmacologic treatment for PD, various complications (such as dyskinesia and motor fluctuations) can occur [3, 4]. Currently, emerging approaches such as exercise, diet, nutritional supplements, and probiotics have shown benefits in PD treatment [5–8]. A low-fat diet, ketogenic diet, and the Mediterranean diet have been shown to be safe therapeutic options for PD [9, 10]. Thus, diet represents a promising and efficient potential therapy for PD patients.

Previously, α-ketoglutarate (AKG), a crucial metabolite in the tricarboxylic acid (TCA) cycle, was shown to

Wenlong Zhang, Liuyan Ding and Mengran Zhang have contributed equally to this work.

✉ Pingyi Xu
pingyixu@sina.com

✉ Yunlong Zhang
ylzhang@gzhmu.edu.cn

1 Department of Neurology, The First Affiliated Hospital of Guangzhou Medical University, Guangzhou 510120, China

2 Key Laboratory of Neuroscience, School of Basic Medical Sciences, Guangzhou Medical University, Guangzhou 511436, China

3 School of Life Sciences, Westlake University, Hangzhou 310024, China

4 Westlake Laboratory of Life Sciences and Biomedicine, Hangzhou 310024, China

5 Institute for Brain Science and Disease, Chongqing Medical University, Chongqing 400016, China

promote the lifespan of *C. elegans*, *S. cerevisiae,* and *Drosophila* [11–13]. Additionally, long-term AKG administration prevented age-related reproductive decline in mice [14]. Recently, an AKG-supplemented diet was reported to suppress frailty and extend longevity in male and female aging mice [15]. Mechanistically, the anti-aging effects of AKG resulted from diverse properties such as anti-oxidative stress effects, regulation of longevity-related mTOR signaling, modulation of epigenetic mechanisms, and anti-inflammatory action [11, 12, 15–18]. Hence, AKG supplementation may function as a potential anti-aging agent. However, evidence showing whether AKG is beneficial in treating the neurodegeneration observed in PD is lacking.

In this study, we report that an AKG-based diet (AKG delivered in the form of a calcium salt, Ca-AKG) significantly ameliorated α-synuclein pathology, and rescued DA neuron degeneration and impaired DA synapses in adeno-associated virus (AAV)-loaded human α-synuclein mice and in transgenic A53T α-synuclein (A53T α-Syn) mice. Mechanistically, we show that the potential mechanisms relied on AKG-mediated enhancement of C1q-mediated autophagy and inhibition of pro-inflammatory events. Moreover, we also determined that the AKG diet increased nigral docosahexaenoic acid (DHA) levels, and DHA supplementation reproduced the anti-α-synuclein effects in the PD mouse model. Furthermore, we revealed that the AKG diet improved the gut microbiota and metabolites in PD mice. Especially, regulating polyunsaturated fatty acid (PUFA) metabolism and microbiota *Lachnospiraceae_NK4A136_group* in the gut-brain axis may underlie AKG's benefits in treating α-synucleinopathy in mice. Ultimately, our findings propose that dietary intake of AKG is a feasible and promising therapeutic approach for PD.

Materials and methods

Reagents

DHA was purchased from GlpBio Technology (Montclair, California, USA). Anti-tyrosine hydroxylase (TH) (F-11, sc-25269) and vGAT (sc-393373) antibodies were purchased from Santa Cruz Biotechnology (Dallas, TX, USA). Anti-synapsin I (#5297), Iba1 (#17198), synaptotagmin (#14558), syntaxin (#18572), and PSD-95 (#3450) antibodies were purchased from Cell Signaling Technology (Danvers, MA, USA). Anti-GAPDH (60004-1) and C1qa (11602-1, used for Western blotting) antibodies were purchased from Proteintech Group (Rosemont, IL, USA). Anti-microtubule-associated protein-1 light chain 3 (LC3) II/I (ab48394), human α-synuclein (ab138501), phospho-α-synuclein (Ser129) (ab51253), C1q (ab71940, used for immunostaining), VMAT2 (ab259970), vGLUT2 (ab216463), and CD68 (ab53444) antibodies were purchased from Abcam (Cambridge, MA, USA). Anti-Iba1 (019–19741) antibody was purchased from FUJIFILM Wako (Osaka, Japan). DyLight 488 goat anti-mouse IgG (H + L) (70-GAM4882 and 70-GAR4882) and DyLight 649 goat anti-rabbit IgG (H + L) (GAM649 and GAR649) antibodies were purchased from Multi Sciences (Hangzhou, China). Anti-rabbit IgG (H + L) (Alexa Fluor® 555 Conjugate, #4413S) and anti-mouse IgG (H + L) (Alexa Fluor® 555 Conjugate, #4409S) were purchased from Cell Signaling Technology (Danvers, MA, USA). Horseradish peroxidase (HRP)-labeled goat anti-rabbit IgG and HRP-labeled goat anti-mouse IgG were purchased from Beyotime Biotechnology (Shanghai, China).

Human α-synuclein preformed fibrils (PFFs) preparation

Purification of human full-length α-synuclein (1–140) was performed as described previously with minor modifications [19, 20]. In brief, the BL21 (DE3) *E. coli* strain (TransGen, Beijing, China) was transformed with a plasmid expressing human full-length α-synuclein. The mixture was shaken at 230 rpm overnight until the optical density reached 0.8 at 600 nm, followed by induction with 1.0 mM isopropyl β-D-thiogalactoside for 4 h. The bacterial pellets were lysed in 50 mM Tris–HCl (pH 7.6), 500 mM NaCl, 1 mM EDTA, 1 mM PMSF, and protease inhibitors, and then sonicated on ice. The lysate was boiled for 10 min, followed by ultracentrifugation at 100,000×*g* for 30 min at 4 °C. After 55% ammonium sulfate precipitation, the protein was purified by anion exchange chromatography (HiTrap column, GE Healthcare, Pittsburgh, PA, USA). The protein was then dialyzed using 10 mM Tris buffer (pH 7.6) and 50 mM NaCl and filtered through a 100-kDa cut-off filter (Amicon Ultra, Millipore, Billerica, MA, USA). Purified protein was used to generate α-synuclein PFFs according to a previous protocol [21]. Purified human α-synuclein was diluted in 10 mM Tris (pH 7.6) and 50 mM NaCl, followed by shaking in a mixer (Eppendorf Thermomixer, Germany) at 1000 rpm for 5–7 days to generate α-synuclein PFFs. Then, the α-synuclein PFFs were probe-sonicated at 20% power for a total of 60 pulses (1 s on and 1 s off). Endotoxin concentration levels of α-synuclein protein and PFFs were determined using an Endotoxin Detection kit (Bioendo Technology, Xiamen, China).

BV2 cell culture and treatment

BV2 cells were cultured in Dulbecco's modified Eagle's medium (GIBCO, Carlsbad, CA, USA) supplemented with 10% fetal calf serum and 1% penicillin/streptomycin at 37 °C in 5% CO_2. To examine the effects of AKG and DHA on PFF-induced endogenous α-synuclein pathology, BV2 cells

were treated with different concentrations (10, 100, 500, and 1,000 μM) of AKG or DHA and PFF (5 μg/ml) for 24 h.

C1qa siRNA transfection

Three siRNAs targeting *C1qa* (siRNA-1, 5′-GGCAATCCA GGCAATATCA-3′; siRNA-2, 5′-ACAGCATCTTCAGCG GATT-3′; siRNA-3, 5′-AGAGTCCATACCAGAACCA-3′) were designed and synthesized by RioBio (Guangzhou, China). Cells were seeded at 80–90% confluence in 6-well plates (Corning, NY, USA) and were transfected with siRNAs. Briefly, siRNAs were diluted to a working concentration of 10 nM in culture medium, mixed with Lipo8000™ Transfection Reagent (Beyotime, Shanghai, China), and incubated for 20 min at room temperature to allow the formation of transfection complexes. The transfection mix was then added to cells in culture plates and incubated for 24 h. Subsequently, cells were incubated with AKG (100 μM), DHA (500 μM), and PFF (5 μg/ml) as indicated for 24 h and were used for immunoblotting and immunofluorescence analysis. The LC3-GFP-RFP lentivirus (HanBio Technology, Shanghai, China) was diluted to 1×10^5 TU/ml to test the effect of *C1qa* siRNA on the formation of autophagosomes and autolysosomes in PFF-treated BV2 cells. As reported previously [22], in the green and red-merged images, autophagosomes are shown as yellow puncta while autolysosomes are shown as red puncta.

Animals

Adult (8-week-old) male C57BL/6 J mice were purchased from SPF Biotechnology Co., Ltd. (Beijing, China). The hSNCA*A53T-Tg mice (also called A53T α-Syn mice) were obtained from the Shanghai Model Organisms Center, Inc (Shanghai, China). According to previous work, homozygous A53T α-Syn Tg mice began to behave neglect of grooming, weight loss, and reduced ambulation beginning at 8 months of age, followed by severe movement dysfunction [23]. To determine the effects of AKG diet on the motor impairment, thus in this study, we selected 8-month-old homozygous A53T α-Syn Tg mice. Age-and sex-matched littermates were used as controls. Animals were housed in a 12 h dark–light cycle with free access to water and food. Animal care and experimental procedures were approved by the guidelines of the Institutional Animal Care and Use Committee of the Guangzhou Medical University and the National Institutes of Health guidelines on the care and use of animals (NIH Publications No. 8023, revised 1978).

AKG diet administration and DHA supplementation

The Calcium Alpha-Ketoglutarate Supplemented Diet (2%, 2918) (TD.160292) and control diet (Teklad-2918) were purchased from Envigo (London, UK). Referring to the effects of AKG in preventing the aging-related events (fertility decline) in mice after 12 weeks' feeding [14], we chose 12 weeks for AKG treatment in this study. After stereotactic injection with the AAV-*h*α-Syn virus, C57BL/6 J mice were fed the Calcium Alpha-Ketoglutarate Supplemented Diet or control diet for three months. Eight-month-old A53T α-Syn mice were fed the Calcium Alpha-Ketoglutarate Supplemented Diet and control diet for three months. DHA was dissolved in a mixture of dimethyl sulfoxide (DMSO) and corn oil, and the concentration of DMSO was less than 0.1%. After stereotactic injection with the AAV-*h*α-Syn virus, mice were intragastrically administrated DHA (160 mg/d/kg) or vehicle for three months, based on a previous study [24]. Then, mice were subjected to behavioral tests and sacrificed for further analysis.

AAV-*h*α-Syn virus generation and stereotactic injection

The AAV-*h*α-Syn virus used in this study has been reported by us and other groups [25, 26]. The AAV9 virus encoding overexpression of either human wild type α-synuclein or green fluorescent protein (AAV-GFP) was driven by the Syn I promoter and enhanced using the woodchuck hepatitis virus posttranscriptional regulatory element (WPRE). Mice were then stereotactically injected bilaterally in the SNpc with either AAV-GFP or AAV-*h*α-Syn-GFP, as stated previously [25]. Briefly, mice were anesthetized and fixed on a stereotactic frame (RWD Life Sciences Corporation, China). AAV-GFP (1.14×10^{12} vg/ml) or AAV-*h*α-Syn -GFP (7.38×10^{12} vg/ml) (packaged by Sunbio Medical Biotechnology, Shanghai, China) (0.5 μl) was delivered into the bilateral SNpc at the target site, as reported previously (Bregma AP, − 3.0 mm, ML, ± 1.3 mm, DV, − 4.7 mm) [25]. The syringe was left in place for 5 min before being slowly withdrawn.

Behavioral tests

Open field test (OFT)

The OFT was performed according to our previous study [25]. The open field test consists of a rectangular plastic box (40 cm × 40 cm × 40 cm) with a center zone. The mice were placed in the center zone and allowed to move freely for 15 min. A video tracking system (EthoVisione XT software, Beijing, China) was used to record the movement tracks of the mice. Then, the total travelled distance, movement speed, and the time the mice spent in the central zone were analyzed.

Pole-climbing test

The pole-climbing test was performed as described previously [27]. The test pole was set at a length of 75 cm and a width of 9 mm. Mice were placed on the top of the pole, and the time it took the mice the reach the ground from the top was recorded.

Rotarod test

The rotarod test was performed as described previously [27]. During the training course, mice were turned on the Rotarod apparatus (Ugo Basile SRL, Gemonio, VA, Italy) at a speed of 10 rpm/min for three days. On the fourth day (test day), the speed of the Rotarod was accelerated from 10 to 40 rpm/min within 5 min, and the latency time the mice took to fall on the Rotarod was recorded.

Grasping test

The grasping test was performed as described previously [27]. The grip test mainly consisted of a 1 mm horizontal metal wire 30 cm above the ground. The mice were allowed to hold the wire with their forelimbs for 10 s. The grasping score was recorded as follows: mice grasping the wire with two hind paws scored 3; mice grasping the wire with one hind paw scored 2; mice that failed to grasp the wire with both hind paws scored 1; mice that fell scored 0.

RNA-sequencing (RNA-seq)

Substantia nigra tissue was collected and the bulk RNA-seq performed. RNA-seq and bioinformatic analysis were performed according to our previous study [27]. Briefly, RNA was isolated using Trizol (Invitrogen, Carlsbad, CA, USA). Sequencing libraries were generated using the NEBNext UltraTM RNA Library Prep Kit for Illumina (NEB, USA) following the manufacturer's recommendations. The mRNA was purified from total RNA using poly-T oligo-attached magnetic beads. PCR products were purified (AMPure XP system) and library quality was assessed on the Agilent Bioanalyzer 2100 system. Sequencing reads were mapped by Novogene (Beijing, China). The DESeq2 R package (1.10.1) was used to statistically analyze the significant differential genes (DEGs). The resulting *p*-values were adjusted using the Benjamini–Hochberg approach to control for false discovery rates. DEGs were defined by an adjusted p value < 0.05 and absolute values of Log_2 (fold change) > 0. The pathways enriched by the DEGs were analyzed using the Kyoto Encyclopedia of Genes and Genomes (KEGG) and Gene Ontology (GO). RNA-seq data used in this study are available under Gene Expression Omnibus database: GSE214446.

Immunohistochemistry and immunofluorescence analysis

Immunohistochemistry and Immunofluorescence were performed as previously described [28]. Fixed brains were dehydrated in 30% sucrose, 0.1 M PBS for 3 days. Coronal slices (30 μm) were cut from frozen tissue using a sliding blade microtome and then blocked with 5% BSA. Slices were incubated with primary antibodies and then incubated with relevant secondary antibodies. For the immunohistochemistry assay, sections were incubated with biotin-conjugated antibody followed by DAB staining using the UltraSensitive SP IHC Kit (MXB biotechnologies, Fuzhou, China). Images were scanned under a microscope (Leica CS2, Hamburg, Germany). For the immunofluorescence assay, nuclei were visualized with DAPI. Fluorescent imaging and data acquisition were performed on a microscope (Leica CS2, Hamburg, Germany). Quantitative analysis was performed using the Image-Pro Plus 6.0 photogram analysis system (IPP 6.0, Media Cybernetics, Bethesda, MD, USA).

Immunoblotting analysis

Brain tissue and cells were collected and total protein was extracted using RIPA Lysis Buffer (Beyotime Biotechnology). Protein samples were then resolved on SDS-PAGE gels followed by electrophoretic transfer onto PVDF membranes. Membranes were blocked with 5% BSA and then incubated with primary antibodies overnight at 4 °C. After incubating with the secondary antibodies conjugated to HRP, the blots were visualized using ECL reagent (Beyotime Biotechnology). Images were captured using the GeneGnome XRQ Chemiluminescence imaging system (Gene Company, Hong Kong, China). Protein bands were quantified by Image J software.

Transmission electron microscopy (TEM)

TEM was performed according to methods from our previous study [28]. Substantia nigra tissues were fixed in 4% paraformaldehyde and 2.5% glutaraldehyde in 0.1 M sodium cacodylate buffer (pH 7.2) and then post-fixed in 1% OsO4 with 1.5% Na ferricyanide in cacodylate buffer. Tissues were stained with 1% tannic acid and 1% uranyl acetate, dehydrated with different concentrations of ethanol, and finally embedded in 100% resin (Sigma, St. Louis, MO, USA). The resin was sectioned using a Leica ultramicrotome and images were captured by transmission electron microscopy (HT7700; Hitachi, Tokyo, Japan).

Quantitative real-time PCR (qRT-PCR)

qRT-PCR was performed according methods from our previous report [27]. Briefly, total RNA was extracted from tissues using Trizol (Invitrogen, Carlsbad, CA, USA). Then, cDNA was generated from 1 μg total RNA using the cDNA Reverse Transcription Kit (Takara, Otsu, Japan). The primers used in this study are listed in Supplementary Table 1.

16S rDNA gene sequencing

16S rDNA gene sequencing was performed as described previously [29]. The bacterial DNA was extracted from fecal samples with a QIAamp Fast DNA stool Mini Kit (Qiagen, Cat# 51604) and PCR amplification was conducted with barcoded specific bacterial primers targeting the variable region 3–4 (V3–V4) of the 16S rRNA gene: forward primer 338F: 5′- ACTCCTACGGGAGGCAGCA-3′ and reverse primer 806R: 5′-GGACTACHVGGGTWTCTAAT-3′. Construction of sequencing libraries and paired- end sequencing was performed on an Illumina NovaSeq6000 platform at Biomarker Technologies Co, Ltd. (Beijing, China) according to standard protocols. Paired-end reads were merged using FLASH v1.2.7 and tags with more than six mismatches were discarded. The merged tags with an average quality score < 20 in a 50 bp sliding window were determined using Trimmomatic, and those shorter than 350 bps were removed. Possible chimeras were further removed and the denoised sequences were clustered into operational taxonomic units (OTUs) with 97% similarity using USEARCH (version 10.0). Taxonomy was assigned to all OTUs by searching the Silva databases (Release128) using QIIME software. Raw sequences were deposited in the Sequence Read Archive database (http://www.ncbinlm.nih.gov/sra). Data statistics were performed on the Biomarker platform (Biomarker Technologies Corporation, China).

Metabolomics analysis

Substantia nigra tissue and faecal samples was collected and the non-targeted metabolomics experiment was carried out by Biomarker Technologies (Beijing, China). After extract buffer was added, the samples were centrifuged and the supernatant was removed for testing. A Waters Xevo G2-XS QTOF high resolution mass spectrometer collected the primary and secondary mass spectrometry data in MSe mode under the control of the acquisition software (MassLynx V4.2, Waters). The low collision energy was 2 V, the high collision energy range was 10–40 V, and the scanning frequency was 0.2 s for a mass spectrum. The parameters of the ESI ion source were as follows: capillary voltage: 2000 V (positive ion mode) or − 1500 V (negative ion mode); cone voltage: 30 V; ion source temperature: 150 °C; desolvent gas temperature 500 °C; backflush gas flow rate: 50 L/h; desolventizing gas flow rate: 800 L/h. Metabolome data statistics were performed on the Biomarker platform (Biomarker Technologies Corporation, China). The screening criteria of differential metabolites were a fold change > 1, p value < 0.05, and VIP > 1. The significance of differential metabolites enriched in the KEGG pathways was calculated using the hypergeometric distribution test. The correlation analysis of the fecal metabolite composition with 16S rDNA gene data was performed on the Biomarker platform (Biomarker Technologies Corporation, China).

Enzyme-linked immunosorbent assay (ELISA)

ELISA was performed as described previously [30]. Briefly, substantia nigra (SN) tissues were homogenized with 0.01 M PBS and centrifuged to obtain the supernatant. Levels of IL-1β, IL-6, and TNF-α were measured using ELISA kits (Shanghai Enzyme-linked Biotechnology, Shanghai, China) according to the manufacturer's instructions. OD values were measured via Multiscan Spectrum (PerkinElmer, MA, USA) at 450 nm, and the results are expressed as pg per mg protein (pg mg^{-1} protein).

Statistical analysis

Statistical analysis was performed using Prism 9.0 (GraphPad Software, La Jolla, CA, USA). One-way analysis of variance (ANOVA) followed by Tukey's *post-hoc* test was used for multiple comparisons. Data are presented as mean ± standard error of the mean (SEM), and the statistical significance level was set at $p < 0.05$.

Results

The AKG diet improves motor dysfunction, α-synuclein pathology, and DA neuron degeneration in AAV-human α-synuclein mice

In this study, we used exogenous AAV-human α-synuclein (AAV-*h*α-Syn) injected mice as α-synucleinopathy model of PD (Fig. 1a). Here, we found that the total travelled distance and movement speed in the open-field test were decreased, the pole-climbing time was increased, in addition, the latency in the rotarod and holding time score were reduced in AAV-*h*α-Syn mice, suggesting the movement impairment in this model (Fig. 1b–g). Besides, AAV-*h*α-Syn increased exogenous human α-synuclein and endogenous phosphorylated α-synuclein (Fig. 1h and i), suggesting this model is typical with α-synuclein pathology. To examine the effects of AKG administration on α-synuclein pathology, we utilized an AKG-based diet containing Ca-AKG

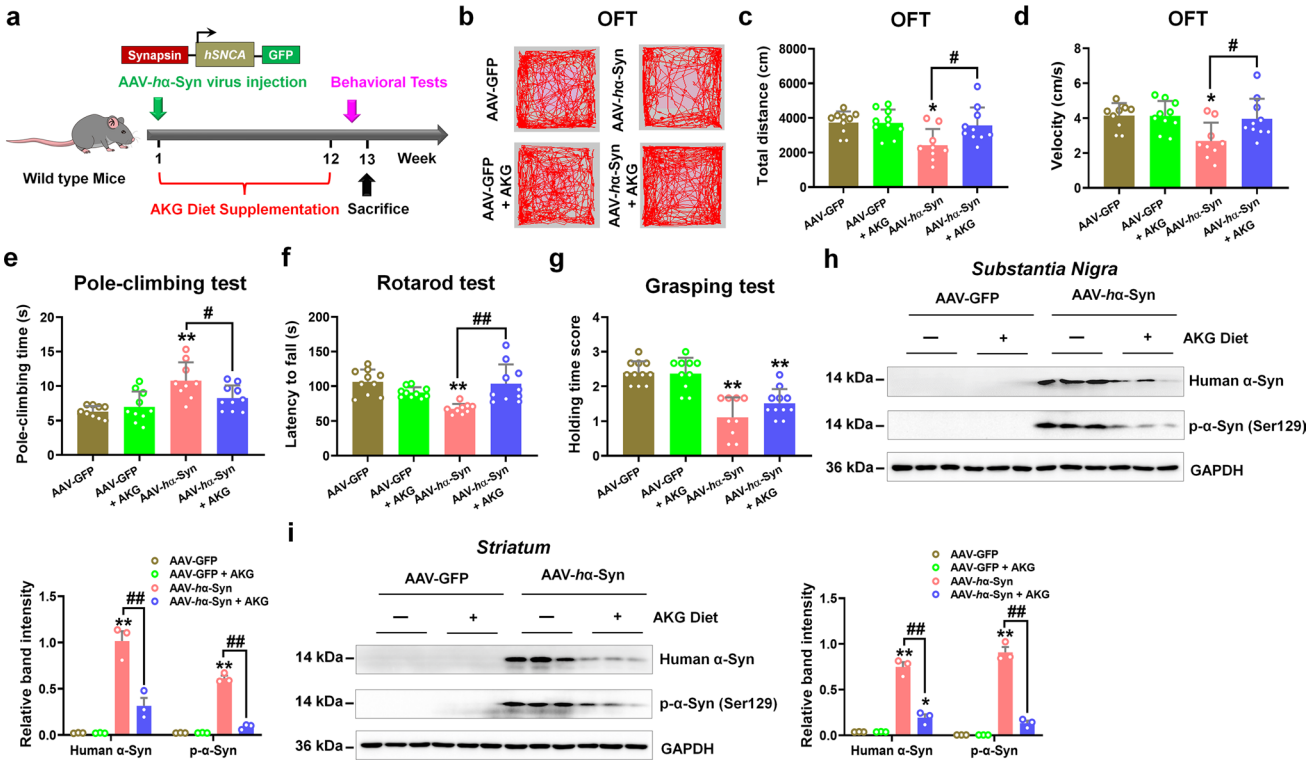

Fig. 1 The AKG diet ameliorates motor dysfunction and α-synuclein pathology in AAV-*h*α-Syn mice. **a** Experimental design for AKG diet administration in AAV-*h*α-Syn mice. **b–d** Representative traces, total travelled distance, and movement speed in the open field test. **e** The pole-climbing test was used to examine bradykinesia in the mice. **f** The rotarod test was used to examine the motor coordination of the mice. **g** The grasping test was used to examine the grip strength of the mice. n = 10, 10, 9 and 10 for AAV-GFP, AAV-GFP + AKG, AAV-*h*α-Syn, and AAV-*h*α-Syn + AKG, respectively. **h** and **i** Representative blots and quantification showing the expression of human α-synuclein and phosphorylated α-synuclein (Ser129) in the SN and striatum. n = 3 per group. Results are expressed as the mean ± SEM. $^{**}p < 0.01$, $^{*}p < 0.05$ vs. AAV-GFP; $^{\#\#}p < 0.01$, $^{\#}p < 0.05$ vs. AAV-*h*α-Syn. Statistical significance was determined using one-way ANOVA and Tukey's test for post hoc comparisons

(named AKG in the figures) [15] in AAV-*h*α-Syn-injected mice for 12 weeks (Fig. 1a). Results showed that in the open field test, the AKG diet promoted total travelled distance and movement speed but not the number of entries to the center zone and time spent in the center (Fig. 1b–d, Supplementary Fig. 1a and b). Additionally, the AKG diet decreased pole-climbing time and improved the behavioral performance in the rotarod test of AAV-*h*α-Syn-injected mice (Fig. 1e and f). The grip strength of the mice was already affected by the expression of AAV-*h*α-Syn, however, it was not rescued by the AKG treatment (Fig. 1g). Intriguingly, the AKG diet nearly abolished the human α-synuclein and phosphorylated α-synuclein in mice injected with AAV-*h*α-Syn in the SN and striatum (Fig. 1h and i).

AAV-*h*α-Syn also damaged nigrostriatal tyrosine hydroxylase (TH, which is the rate-limiting enzyme in the biosynthesis of dopamine) expression, reduced the number of synaptic vesicles and vesicular monoamine transporter 2 (VMAT2, which regulates dopamine release) in TH-positive cells in the SN and decreased expression of synaptic protein (syntaxin) in the striatum (Fig. 2a–f). Whilst, AKG diet rescued the nigrostriatal DA neuron death in mice injected with AAV-*h*α-Syn (Fig. 2a–c). Furthermore, the AKG diet increased the number of synaptic vesicles without affecting its diameter (Fig. 2d, Supplementary Fig. 2). In addition, AKG promoted VMAT2-positive rather than vesicular GABA transporter (vGAT, inhibitory neuron marker) or vesicular glutamate transporter 2 (vGLUT2, excitatory neuron marker)-positive neurons in the SN of mice injected with AAV-*h*α-Syn (Fig. 2e, Supplementary Fig. 3a and b). Because DA neurons in the SN project to the dorsal putamen of the striatum, we found AAV-*h*α-Syn decreased the expression of syntaxin in the striatum as compared with AAV-GFP (Fig. 2f). AKG diet increased synaptic proteins such as synapsin and syntaxin in the striatum of mice injected with AAV-*h*α-Syn (Fig. 2f).

These data suggest that AKG diet attenuates α-synuclein pathology, DA neuron loss and behavioral impairment in mice injected with AAV-*h*α-Syn.

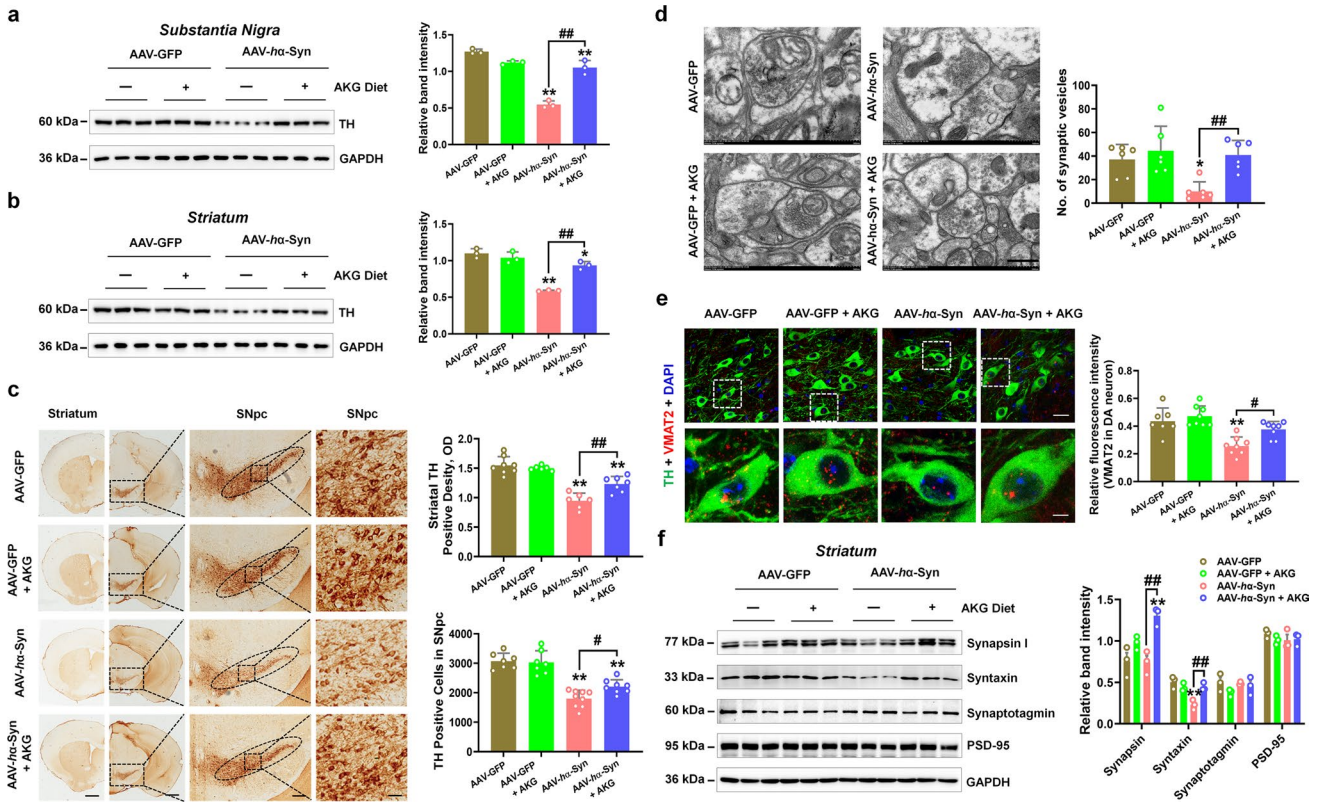

Fig. 2 The AKG diet attenuates DA neuron death in AAV-*h*α-Syn mice. **a** and **b** Representative blots and quantification showing TH expression in the SN and striatum. n = 3 per group. **c** Immunohistochemistry staining and quantification of TH-positive cells in SNpc and TH-positive density in the striatum. Scale bars, 1 mm for striatum, 800 μm for SNpc. Magnified images of TH-positive cells in the SNpc are shown in the right column of the panel. n = 6–9. Scale bars, 100 μm. **d** Quantitative analysis and the representative images of ultrastructural synaptic vesicles in the SN. n = 6 per group. Scale bar, 500 μm. **e** Immunofluorescence staining and quantification of VMAT2 within TH-positive cells in the SN of AAV-GFP, AAV-GFP + AKG, AAV-*h*α-Syn, and AAV-*h*α-Syn + AKG groups. Scale bars, 40 μm. Magnified images are shown in the bottom row. Scale bars, 10 μm. n = 7–8. **f** Representative blots and quantification showing the expression of Synapsin, Syntaxin, Synaptotagmin, and PSD-95 in the striatum. n = 3 per group. Results are expressed as the mean ± SEM. $^{**}p < 0.01$, $^{*}p < 0.05$ vs. AAV-GFP; $^{\#\#}p < 0.01$, $^{\#}p < 0.05$ vs. AAV-*h*α-Syn. Statistical significance was determined using one-way ANOVA and Tukey's test for post hoc comparisons

The AKG diet increases nigral DHA levels in the PD model

We next determined a metabolic mechanism by which the AKG diet ameliorated the α-synuclein pathology. First, we identified the differential metabolites and their enriched pathways between the AAV-GFP and AAV-GFP + AKG, AAV-GFP and AAV-*h*α-Syn, AAV-*h*α-Syn and AAV-*h*α-Syn + AKG groups in substantia nigra tissue (Supplementary Figs. 4, 5, 6). The distribution of metabolites, PCA plot, and relative abundance of metabolites from the AAV-GFP, AAV-*h*α-Syn and AAV-*h*α-Syn + AKG groups are shown in Fig. 3a–c and Supplementary Fig. 7a. Notably, we identified DHA and Pyruvic acid as metabolites affected by the AKG diet, as they were decreased in the AAV-*h*α-Syn group compared with the AAV-GFP group (Fig. 3d–f, Supplementary Fig. 7b–j). In addition, we showed that the differential metabolites upon AKG diet supplementation in AAV-*h*α-Syn mice participated in "Alpha Linolenic Acid and Linoleic Acid Metabolism" (Fig. 3g).

Given that DHA has been proved to exert neuroprotection in 6-hydroxydopamine (6-OHDA) and rotenone-induced PD animal models [31–33], we then tested its effects on α-synuclein pathology. After DHA administration for 12 weeks, we found that DHA decreased pole-climbing time and increased motor coordination in the rotarod test and grip strength in the grasping test of mice injected with AAV-*h*α-Syn (Fig. 4a–d). Additionally, DHA treatment reduced the exogenous human α-synuclein and endogenous phosphorylation of α-synuclein (Fig. 4e). DHA administration also rescued nigrostriatal DA neuron loss in the mice injected with AAV-*h*α-Syn (Fig. 4f–h). Hence, these results reveal that AKG diet increases DHA concentration and DHA exerts neuroprotection in the AAV-*h*α-Syn mice.

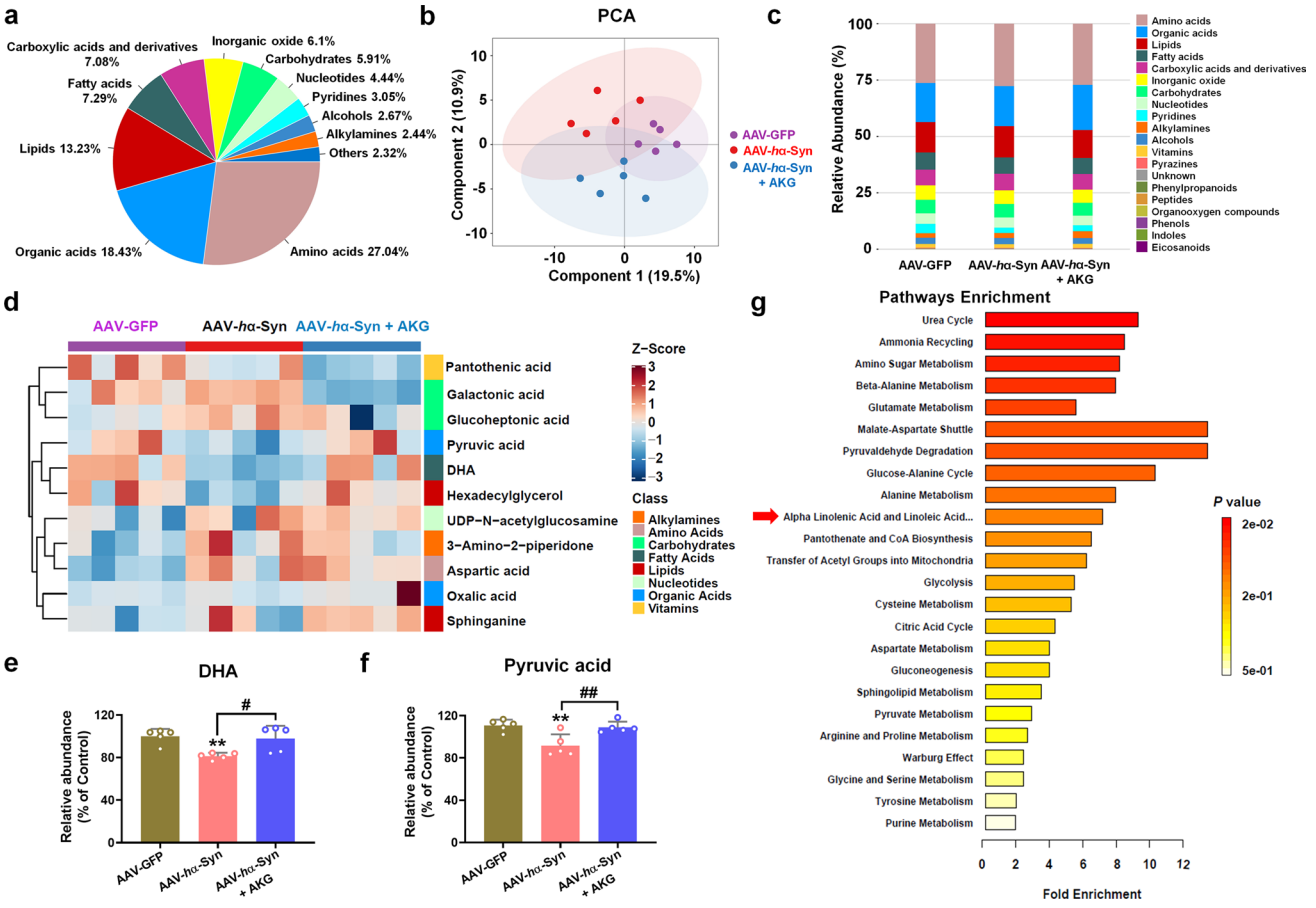

Fig. 3 The AKG diet increases nigral DHA concentrations in AAV-*h*α-Syn mice. **a**–**c** The distribution of metabolites, PCA plot and relative abundance of metabolites in the AAV-GFP, AAV-*h*α-Syn, and AAV-*h*α-Syn + AKG groups. n = 5 per group. **d** The metabonomic analysis of differential metabolite expression in the AAV-GFP, AAV-*h*α-Syn, and AAV-*h*α-Syn + AKG groups. **e** and **f** The expression of DHA and Pyruvic acid in the SN of the AAV-GFP, AAV-*h*α-Syn, and AAV-*h*α-Syn + AKG groups. n = 5 per group. **g** KEGG pathways enriched by these differential metabolites. Results are expressed as the mean ± SEM. $^{**}p < 0.01$ vs. AAV-GFP; $^{\#\#}p < 0.01$, $^{\#}p < 0.05$ vs. AAV-*h*α-Syn. Statistical significance was determined using one-way ANOVA and Tukey's test for post hoc comparisons

AKG and DHA regulate α-synuclein degradation via C1qa-mediated autophagy

We then employed RNA-seq to explore the mechanism behind the anti-PD effects of AKG. We found that the AKG diet increased the expression of 1,073 genes and decreased the expression of 527 genes compared with AAV-GFP (Supplementary Fig. 8a and b). The upregulated differential genes (DEGs) were enriched in the KEGG pathways such as "Glutamatergic synapse", "Long-term potentiation", and "Axon guidance"; the downregulated DEGs were enriched in "Parkinson's disease", "Alzheimer's disease (AD)", and "Antigen processing and presentation" pathways (Supplementary Fig. 8c and d). These results suggest that AKG affected the signaling pathways related to neurodegenerative diseases. Moreover, the AKG diet upregulated 38 genes in AAV-*h*α-Syn mice which were decreased in AAV-*h*α-Syn mice compared with AAV-GFP (Fig. 5a–c, Supplementary Fig. 9). These 38 DEGs were enriched in the KEGG pathways such as "Complement and coagulation cascades", "Parkinson's disease", and "Alzheimer's disease"; various representative genes are listed (Fig. 5d and e). Because genes like *C1qa*, *C1qb*, *C1qc,* and *C4b* were enriched in the top4 KEGG pathways, we further confirmed their expression by qRT-PCR (Fig. 5f and g). Since microglia is the main source of C1q[34], and C1q has been shown to enhance the microglial phagocytosis of misfolded proteins like Aβ [35–37]; we found that AKG decreased phosphorylated α-synuclein and increased C1q within microglia in the SNpc of AAV-*h*α-Syn mice (Fig. 5h and i). Although neuronal phosphorylated α-synuclein was also decreased (Supplementary Fig. 10), we did not find C1q signals in neuron (Supplementary Fig. 11).

We then ask whether the removed phosphorylated α-synuclein was mediated by C1q-induced autophagy. Firstly, we found that AKG and DHA treatment increased the expression of LC3 in the SN of AAV-GFP and AAV-*h*α-Syn

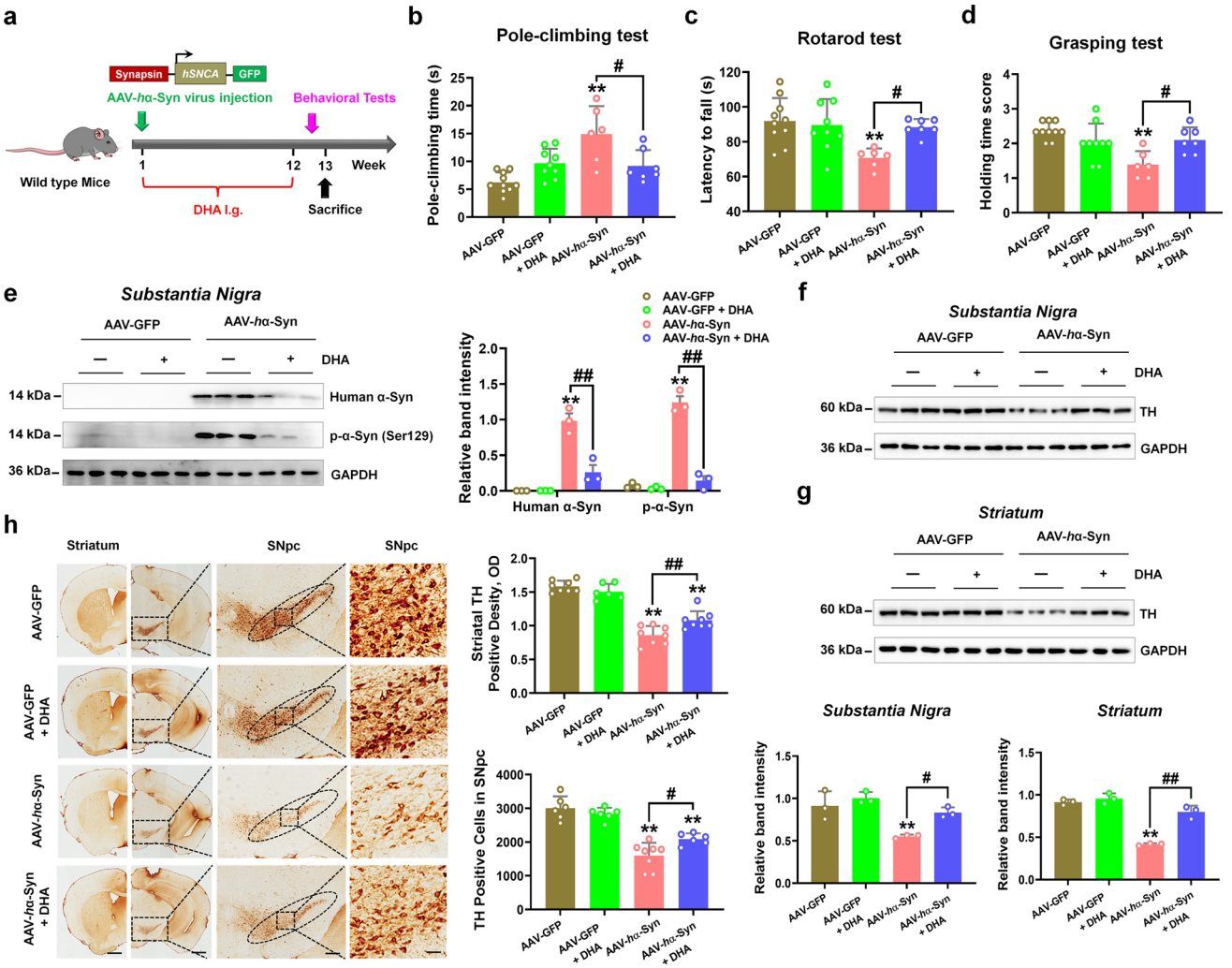

Fig. 4 DHA improves movement disorder, α-synuclein pathology, and DA neuron loss in AAV-*h*α-Syn mice. **a** Experimental design for DHA supplementation in AAV-*h*α-Syn mice. **b** The pole-climbing test was used to examine bradykinesia in the mice. **c** The rotarod test was used to examine the motor coordination of the mice. **d** The grasping test was used to examine the grip strength of the mice. n = 10, 9, 6 and 7 for AAV-GFP, AAV-GFP + DHA, AAV-*h*α-Syn, and AAV-*h*α-Syn + DHA, respectively. **e** Representative blots and quantification showing the expression of human α-synuclein and phosphorylated α-synuclein (Ser129) in the SN. n = 3 per group. **f** and **g** Representative blots and quantification showing TH expression in the SN and striatum. n = 3 per group. **h** Immunohistochemistry staining and quantification of TH-positive cells in SNpc and TH-positive density in the striatum. Scale bars, 1 mm for striatum, 800 μm for SNpc. Magnified images of TH-positive cells in the SNpc are shown in the right column of the panel. n = 6–8. Scale bars, 100 μm. Results are expressed as the mean ± SEM. $^{**}p < 0.01$ vs. AAV-GFP; $^{\#\#}p < 0.01$, $^{\#}p < 0.05$ vs. AAV-*h*α-Syn. Statistical significance was determined using one-way ANOVA and Tukey's test for post hoc comparisons

mice (Fig. 6a–d), suggesting that AKG and DHA actually induced autophagy in the AAV-*h*α-Syn mice. Afterwards, we treated microglial BV2 cells with human α-synuclein PFF and different concentrations of AKG and DHA and found that AKG (100–1000 μM) and DHA (500 and 1000 μM) significantly decreased endogenous phosphorylated α-synuclein (Supplementary Fig. 12). Then, we examined whether AKG and DHA affect autophagy, and chose 100 μM AKG and 500 μM DHA for these experiments. Results showed that AKG and DHA increased the LC3 II/I ratio and C1q expression in PFF-treated BV2 cells (Fig. 6e and f), suggesting both AKG and DHA enhanced the autophagy of BV2 cells. To explore whether AKG and DHA-regulated autophagy is mediated by C1q, we screened siRNAs targeting *C1qa* and selected the third sequence (Supplementary Fig. 13). Intriguingly, *C1qa* knockdown abolished AKG and DHA-induced α-synuclein degradation via autophagy (Fig. 6g and h). Additionally, *C1qa* knockdown also counteracted AKG and DHA-enhancement of the number of autophagosomes and autolysosomes in PFF-treated BV2 cells (Fig. 6i and j). These results reveal that AKG and DHA regulate autophagy-dependent α-synuclein degradation via C1qa.

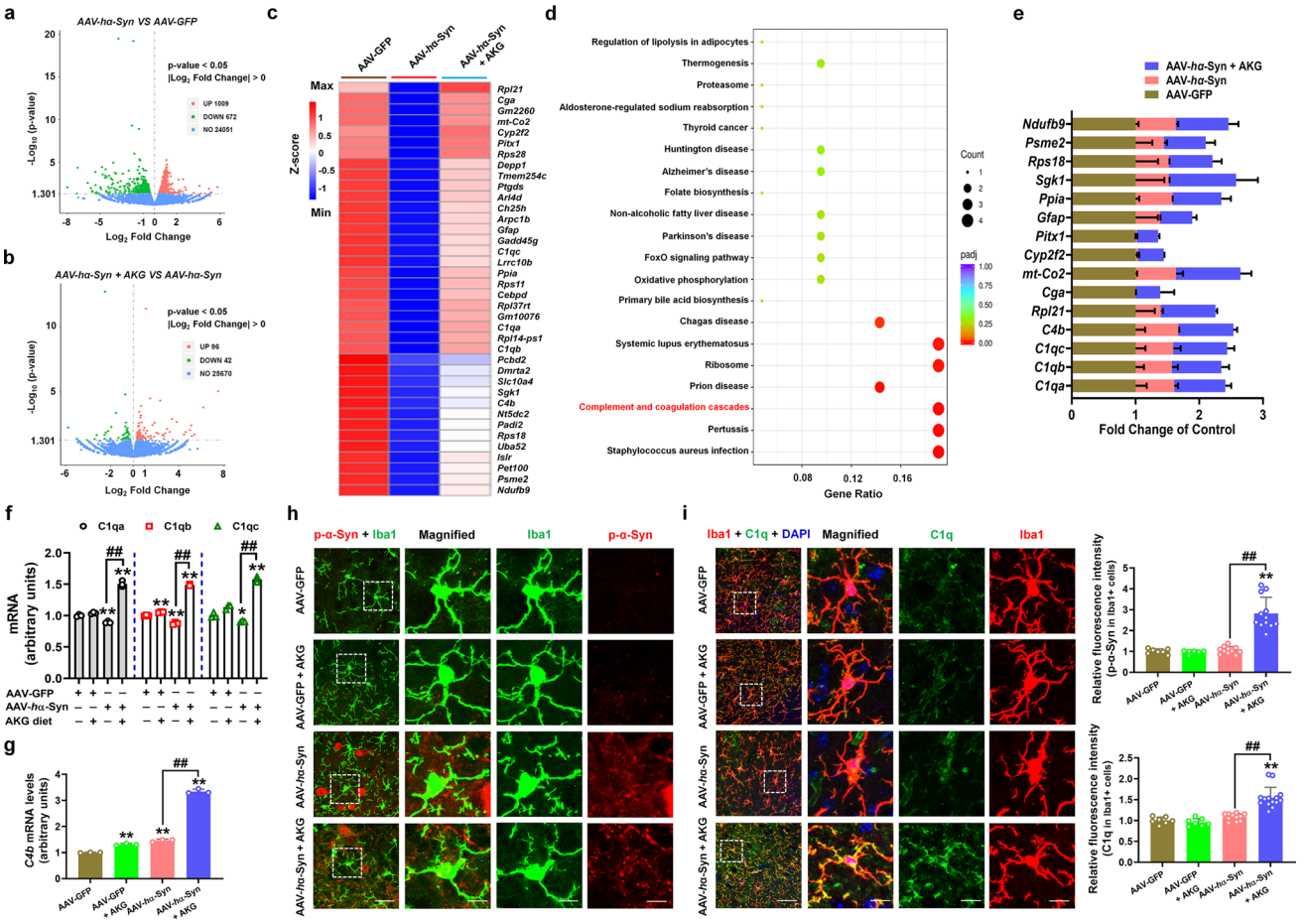

Fig. 5 RNA-seq profile of AKG diet administration in AAV-*h*α-Syn mice. **a** and **b** Volcano plot showing the DEGs between AAV-*h*α-Syn and AAV-GFP, AAV-*h*α-Syn + AKG, and AAV-*h*α-Syn. **c** AKG diet reversed DEGs which were decreased by AAV-*h*α-Syn compared with AAV-GFP. **d** The KEGG pathways enriched by the AKG diet reversed DEGs in (**c**). "Complement and coagulation cascades" pathway is highlighted in red. **e** The expression of representative DEGs reversed by the AKG diet in AAV-GFP, AAV-*h*α-Syn, and AAV-*h*α-Syn + AKG. **f** and **g** The mRNA expression levels of *C1qa*, *C1qb*, *C1qc,* and *C4b* in the AAV-GFP, AAV-GFP + AKG, AAV-*h*α-Syn, and AAV-*h*α-Syn + AKG groups. n = 3 per group. **h** Immunofluorescence staining and quantification of phosphorylated α-synuclein within Iba1-positive cells in the SN of AAV-GFP, AAV-GFP + AKG, AAV-*h*α-Syn, and AAV-*h*α-Syn + AKG groups. Scale bars, 40 μm. Magnified images are shown in the bottom row. Scale bars, 10 μm. n = 6–12. **i** Immunofluorescence staining and quantification of C1q within Iba1-positive cells in the SN of AAV-GFP, AAV-GFP + AKG, AAV-*h*α-Syn, and AAV-*h*α-Syn + AKG groups. Scale bars, 40 μm. Magnified images are shown in the bottom row. Scale bars, 10 μm. n = 7–14. Results are expressed as the mean ± SEM. $^{**}p < 0.01$, $^{*}p < 0.05$ vs. AAV-GFP; $^{\#\#}p < 0.01$, $^{\#}p < 0.05$ vs. AAV-*h*α-Syn. Statistical significance was determined using one-way ANOVA and Tukey's test for post hoc comparisons

AKG and DHA prevent pro-inflammatory response in AAV-human α-synuclein mice

Since ectogenic α-synuclein has been reported to induce pro-inflammatory response [38, 39], we also revealed that AAV-*h*α-Syn elicited the mRNA and protein expressions of pro-inflammatory cytokines (IL-1β, IL-6 and TNF-α) in the SN (Fig. 7a–e). In the AAV-*h*α-Syn group, the endpoint voxels and branch length were decreased, while the cellular volume of Iba1 + cells were increased (Fig. 7f and g), suggesting microglia change from a "resting" ramified phenotype to an "activated" bushy phenotype. We found that the AKG diet decreased mRNA expression of the pro-inflammatory cytokines *Il-1b*, *Il-6*, *Tnfa*, *Ifng* and the microglial markers *Cx3cr1* and *P2ry12* (Fig. 7a and b). The AKG diet suppressed the IL-1β and IL-6 protein levels, while it showed no obvious effects on TNF-α in the SN of AAV-*h*α-Syn mice (Fig. 7c). DHA treatment inhibited the mRNA levels of *Il-1b*, *Il-6*, and *Tnfa*, and their protein (IL-1β, IL-6 and TNF-α) expressions in the SN of AAV-*h*α-Syn mice (Fig. 7d and e). Besides, AKG and DHA treatment increased the endpoint voxels and branch length, and decreased the cellular volume of Iba1 + cells in the SN of AAV-*h*α-Syn mice, indicating microglia are deactivated in the presence of AKG and DHA (Fig. 7f and g). AKG and DHA also suppressed the expression of CD68 (a classic maker for microglial activation) in AAV-*h*α-Syn mice,

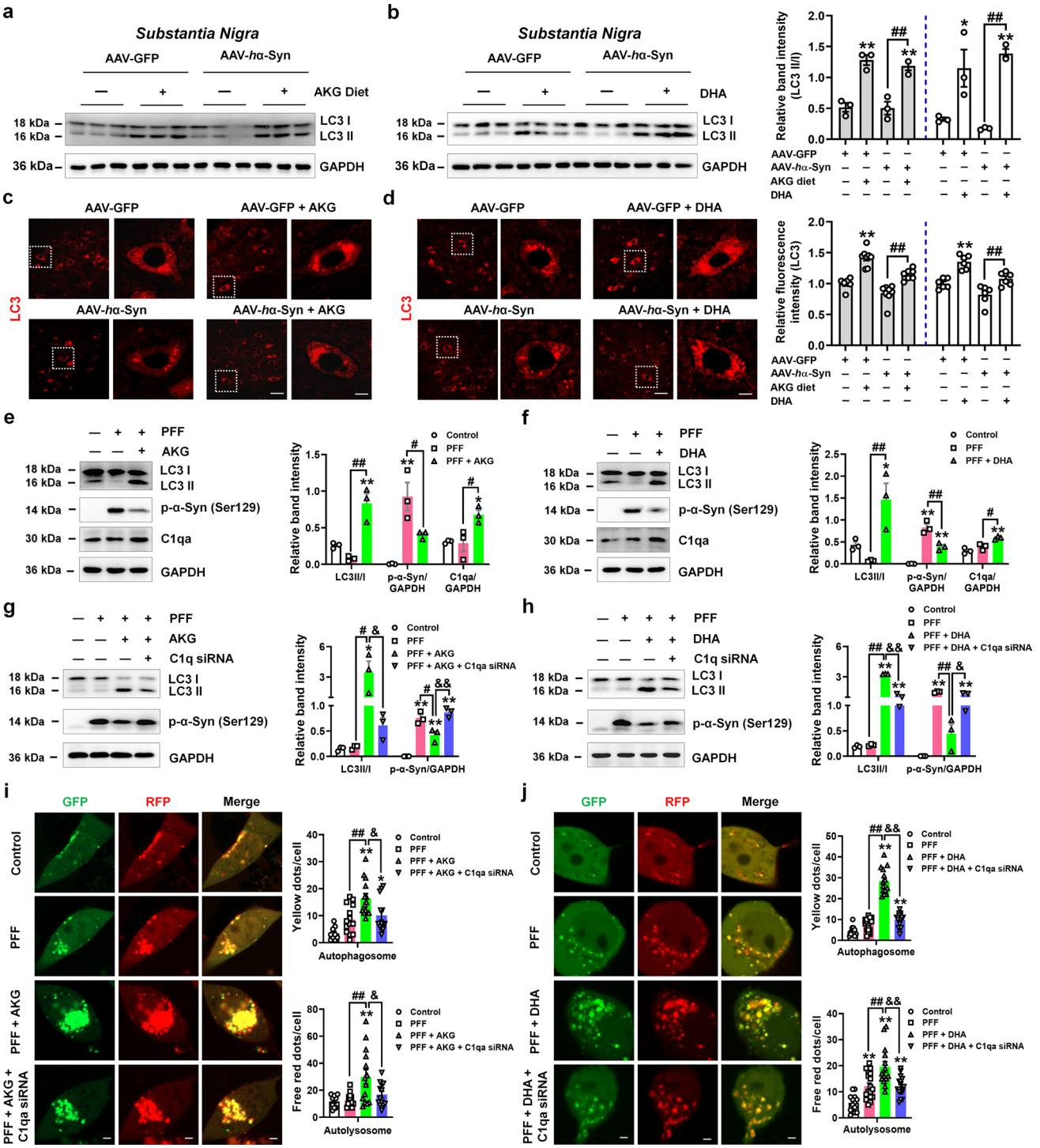

Fig. 6 AKG and DHA regulate α-synuclein degradation via C1qa. **a** and **b** Representative blots and quantification showing the expression of LC3 in the SN of AAV-GFP and AAV-*h*α-Syn mice treated with AKG or DHA. n = 3 per group. **c** and **d** Immunofluorescence staining and quantification of LC3 in the SN of AAV-GFP and AAV-*h*α-Syn mice treated with AKG or DHA. Scale bars, 40 μm. Magnified images are shown in the right row. Scale bars, 8 μm. n = 6–8. **e** and **f** Representative blots and quantification showing the expression of LC3, phosphorylated α-synuclein (Ser129), and C1qa in BV2 cells treated with PFF and different concentrations of AKG (**e**) and DHA (**f**). n = 3. **g** and **h** Representative blots and quantification showing the expression of LC3 and phosphorylated α-synuclein (Ser129) in BV2 cells treated with PFF, AKG, or DHA and C1qa siRNA. n = 3. **i** and **j** Immunofluorescence staining and quantification of LC3-GFP-RFP in BV2 cells treated with PFF, AKG, or DHA and C1qa siRNA. In the merged images, yellow dots represent the formation of autophagosomes and red dots represent the formation of autolysosomes. Scale bars, 2.5 μm. n = 9–18. Results are expressed as the mean ± SEM. $^{**}p < 0.01$, $^{*}p < 0.05$ vs. AAV-GFP or Control; $^{\#\#}p < 0.01$, $^{\#}p < 0.05$ vs. AAV-*h*α-Syn or PFF; $^{\&\&}p < 0.01$, $^{\&}p < 0.05$ vs. PFF + AKG or DHA. Statistical significance was determined using one-way ANOVA and Tukey's test for post hoc comparisons

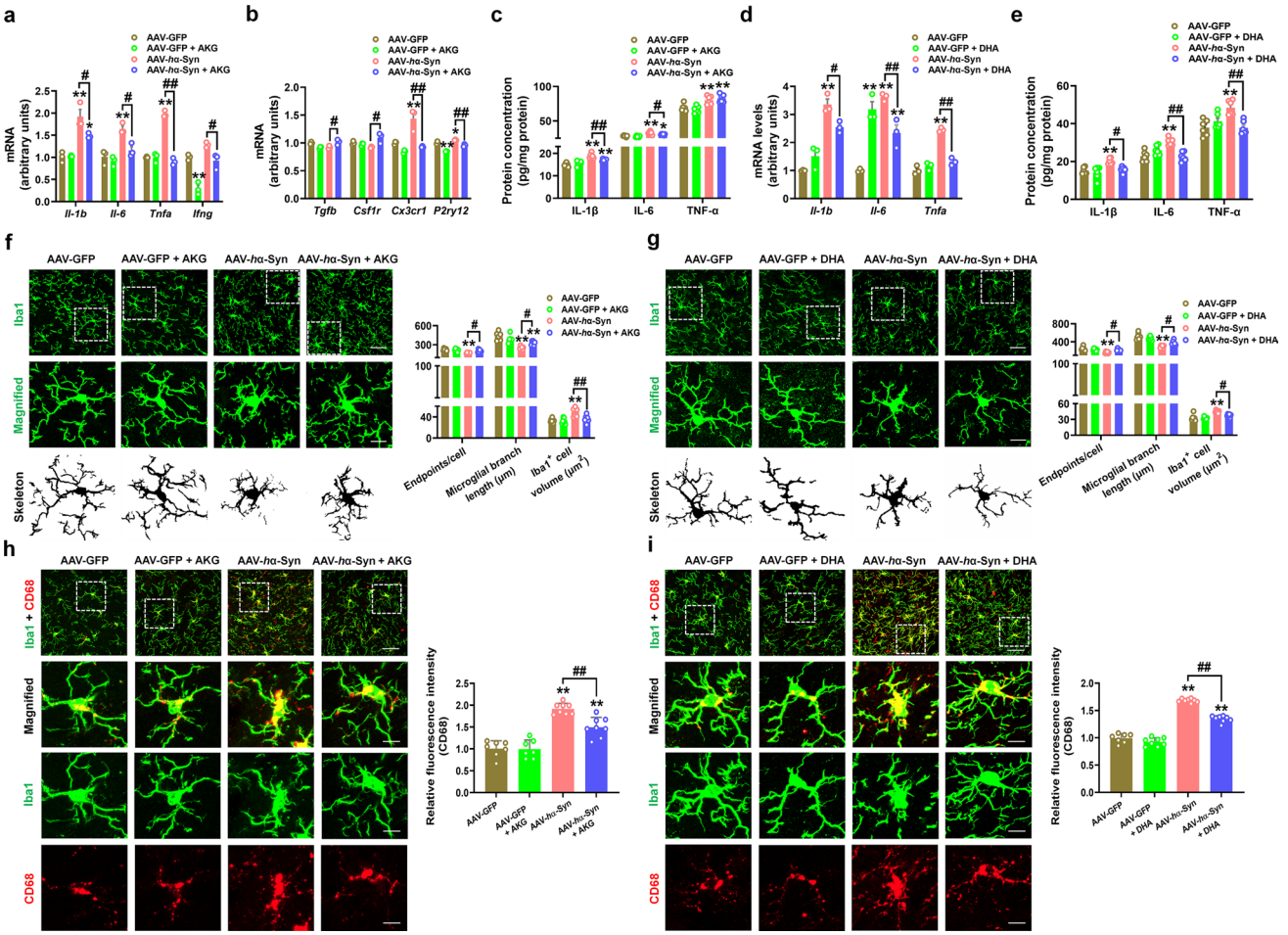

Fig. 7 AKG and DHA suppress pro-inflammatory response in AAV-*h*α-Syn mice. **a** and **b** The mRNA expression levels of *Il-1b*, *Il-6*, *Tnfa*, *Ifng*, *Tgfb*, *Csf1r*, *Cx3cr1,* and *P2ry12* in the AAV-GFP, AAV-GFP + AKG, AAV-*h*α-Syn, and AAV-*h*α-Syn + AKG groups. n = 3 per group. **c** The protein expression of IL-1β, IL-6, and TNF-α in the SN were determined by ELISA. n = 6 per group. **d** The mRNA expression levels of *Il-1b*, *Il-6*, and *Tnfa* in the AAV-GFP, AAV-GFP + DHA, AAV-*h*α-Syn, and AAV-*h*α-Syn + DHA groups. n = 3 per group. **e** The protein expression of IL-1β, IL-6, and TNF-α in the SN were determined by ELISA. n = 6 per group. **f** Immunofluorescence staining and quantification of endpoint voxels, branch length, and volume of Iba1-positive cells in the SN of AAV-GFP, AAV-GFP + AKG, AAV-*h*α-Syn, and AAV-*h*α-Syn + AKG groups. Scale bars, 40 μm. Magnified images are shown in the bottom row. Scale bars, 10 μm. n = 6–7. **g** Immunofluorescence staining and quantification of endpoint voxels, branch length, and volume of Iba1-positive cells in the SN of AAV-GFP, AAV-GFP + DHA, AAV-*h*α-Syn, and AAV-*h*α-Syn + DHA groups. Scale bars, 40 μm. Magnified images are shown in the bottom row. Scale bars, 10 μm. n = 6 per group. **h** Immunofluorescence staining and quantification of CD68 in the SN of AAV-GFP, AAV-GFP + AKG, AAV-*h*α-Syn, and AAV-*h*α-Syn + AKG groups. Scale bars, 40 μm. Magnified images are shown in the bottom row. Scale bars, 10 μm. n = 7–8. **i** Immunofluorescence staining and quantification of CD68 in the SN of AAV-GFP, AAV-GFP + DHA, AAV-*h*α-Syn, and AAV-*h*α-Syn + DHA groups. Scale bars, 40 μm. Magnified images are shown in the bottom row. Scale bars, 10 μm. n = 7–8. Results are expressed as the mean ± SEM. $^{**}p < 0.01$, $^{*}p < 0.05$ vs. AAV-GFP; $^{\#\#}p < 0.01$, $^{\#}p < 0.05$ vs. AAV-*h*α-Syn. Statistical significance was determined using one-way ANOVA and Tukey's test for post hoc comparisons

which further support their anti-inflammatory effects (Fig. 7h and i). Thus, these findings indicate that the AKG diet and DHA treatment attenuated pro-inflammatory response in mice injected with AAV-*h*α-Syn.

AKG supplementation modulates gut microbiota and microbial metabolites in AAV-human α-synuclein mice

Because the gut microbiota and microbial metabolism play important roles in α-synuclein pathology in PD [40, 41],

we then test whether the AKG diet regulates the microbial metabolism pathway. Firstly, we compared the microbial metabolites between the AAV-GFP + AKG and AAV-GFP groups and consistently found that these differential metabolites were enriched in the "Alpha Linolenic acid metabolism" and "Linoleic acid Metabolism" KEGG pathways (Supplementary Fig. 14a–f). Then we showed that the AAV-*h*α-Syn group had 193 increased and 207 decreased microbial metabolites compared with the AAV-GFP group in faecal samples (Fig. 8a and b), and we identified several metabolites that were altered between the AAV-*h*α-Syn and AAV-GFP groups (Fig. 8c). The AKG diet exerted significant effects on the microbial metabolites compared with AAV-*h*α-Syn mice fed the standard diet, increasing 616 and decreasing 985 metabolites (Fig. 8d and e). The differential metabolites between AAV-*h*α-Syn and AAV-GFP, AAV-*h*α-Syn + AKG, and AAV-*h*α-Syn are shown (Fig. 8f). The AKG diet significantly affected metabolite abundance; AKG reversed decreases in 11-dehydro-thromboxane B2 in the AAV-*h*α-Syn group compared with the AAV-GFP group (Fig. 8g). In the treatment group, AKG further increased leukotriene E4 and decreased PC [14:0/20:4(8Z,11Z,14Z,17Z)] and 6-keto-prostaglandin F1a compared with the AAV-*h*α-Syn or AAV-GFP groups (Fig. 8g). Moreover, we found

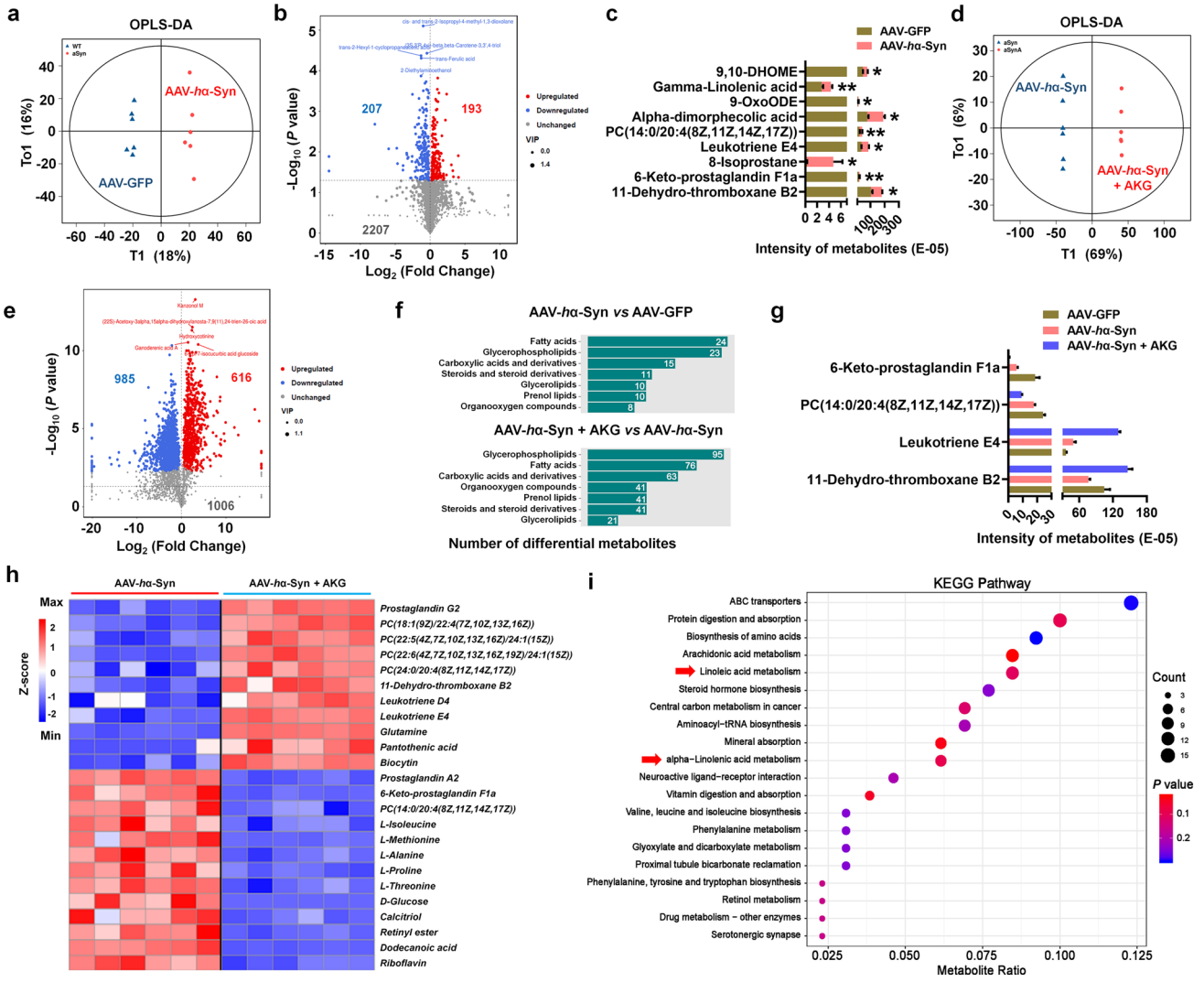

Fig. 8 The AKG diet alters the microbial metabolites in AAV-*h*α-Syn mice. **a** and **b** OPLS-DA plot and volcano plot showing the differential metabolites between AAV-*h*α-Syn and AAV-GFP. n = 6 per group. **c** The expression pattern of differential metabolites between AAV-*h*α-Syn and AAV-GFP. **d** and **e** OPLS-DA plot and volcano plot showing the differential metabolites between AAV-*h*α-Syn + AKG and AAV-*h*α-Syn. n = 6 per group. **f** The metabolomic class enriched by the differential metabolites between AAV-*h*α-Syn and AAV-GFP, AAV-*h*α-Syn + AKG and AAV-*h*α-Syn. **g** The expression pattern of differential metabolites among AAV-GFP, AAV-*h*α-Syn, and AAV-*h*α-Syn + AKG. **h** Hierarchical clustering of differential metabolites between AAV-*h*α-Syn + AKG and AAV-*h*α-Syn. **i** KEGG pathway enriched by these differential metabolites in (**h**). "Linoleic Acid Metabolism" and "Alpha Linolenic Acid metabolism" are highlighted

that the AKG diet increased the abundance of prostaglandin G2, leukotriene D4, leukotriene E4, and several lipids, and decreased prostaglandin A2, 6-keto-prostaglandin F1a, and several amino acids such as L-isoleucine, L-methionine, and L-alanine in AAV-*h*α-Syn mice (Fig. 8h). These altered microbial metabolites were enriched in KEGG pathways such as "Serotonergic synapse" and "Drug metabolism" (Fig. 8i, Supplementary Fig. 15). Intriguingly, we also found the AKG diet altered the "Alpha Linolenic acid metabolism" and "Linoleic acid Metabolism" pathways in AAV-*h*α-Syn mice (Fig. 8i), which was consistent with the pathways enriched by AKG-modulated nigral metabolites.

We further examined the gut microbiota and found that the AKG diet slightly reduced several α-diversity indicators

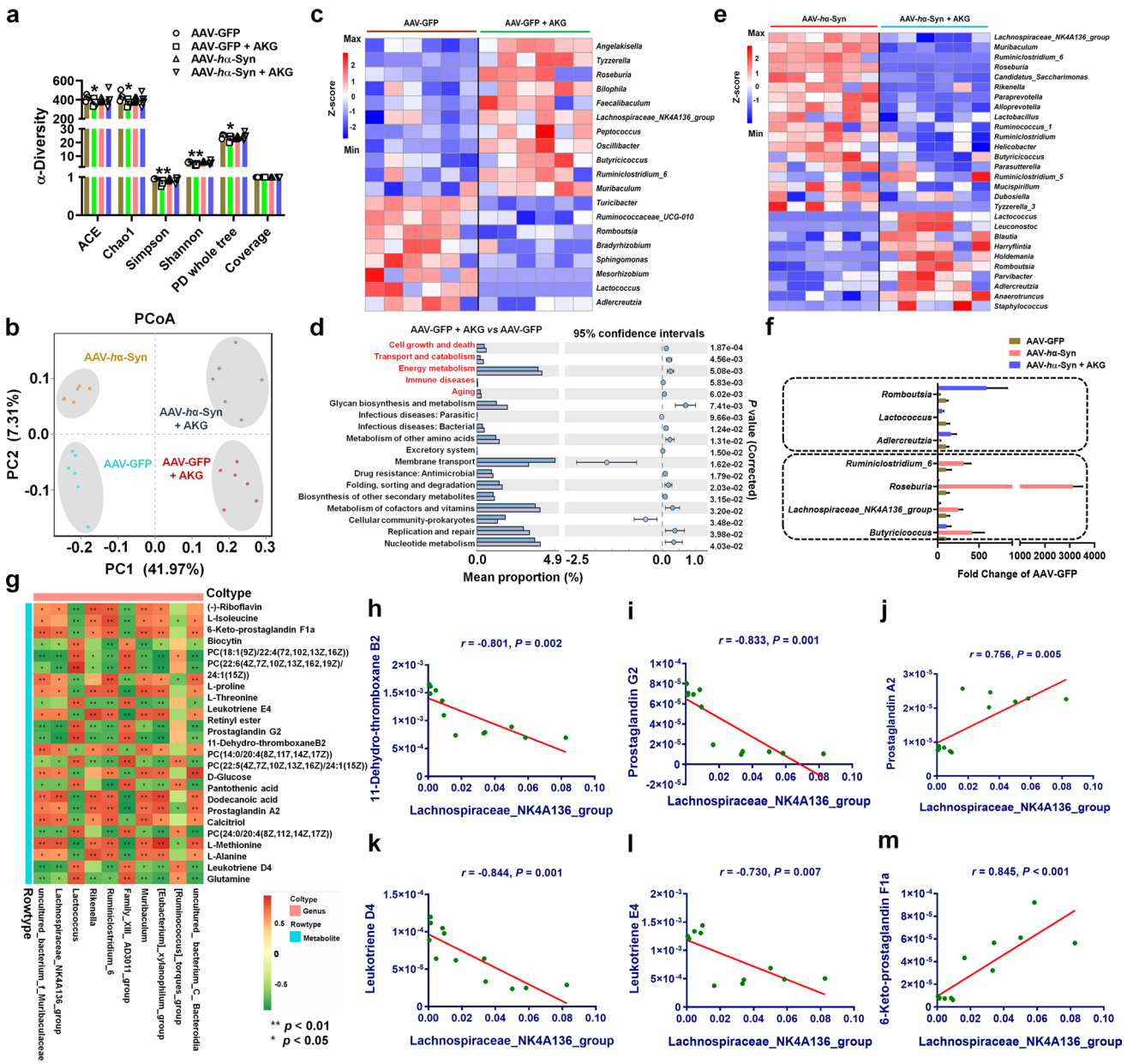

Fig. 9 The AKG diet regulates the gut microbiota in AAV-*h*α-Syn mice. **a** and **b** The expression of α-diversity indicators (ACE, Chao1, Simpson, Shannon, PD whole tree and Coverage) and PCoA plot in the AAV-GFP, AAV-GFP + AKG, AAV-*h*α-Syn, and AAV-*h*α-Syn + AKG groups. n = 6 per group. **c** Hierarchical clustering of differential gut microbiota between AAV-GFP + AKG and AAV-GFP. **d** The KEGG pathways enriched by the differential gut microbiota in (**c**). **e** Hierarchical clustering of differential gut microbiota between AAV-*h*α-Syn + AKG and AAV-*h*α-Syn. **f** The AKG diet reversed AAV-*h*α-Syn-increased or -decreased gut microbiota compared with AAV-GFP. **g** The correlation analysis of differential gut microbiota and microbial metabolites. **h**–**m** The correlation between *Lachnospiraceae_NK4A136_group* and 11-Dehydro-thromboxane B2 (**h**), Prostaglandin G2 (**i**), Prostaglandin A2 (**j**), Leukotriene D4 (**k**), Leukotriene E4 (**l**), and 6-Keto-prostaglandin F1a (**m**)

such as ACE, Chao1, Simpson, Shannon, and PD whole tree compared with the AAV-GFP group (Fig. 9a). The PCoA plot, multi-sample Shannon curves, non-metric multidimensional scaling (NMDS), and individual composition of the gut microbiota from these four groups are shown in Fig. 9b and Supplementary Fig. 16a–c. The top 5 pathways enriched by differential gut microbiota from AKG diet intervention in wild-type mice were "Cell growth and death", "Transport and catabolism", "Energy metabolism", "Immune diseases", and "Aging" (Fig. 9c and d). We also showed the differential gut microbiota between AAV-*h*α-Syn + AKG and AAV-*h*α-Syn at the genus level (Fig. 9e), and the AKG diet reversed the AAV-*h*α-Syn- induced increases in *Butyricicoccus*, *Lachnospiraceae_NK4A136_group*, *Roseburia*, *Ruminiclostridium_6*, and AAV-*h*α-Syn-decreases in *Adlercreutzia*, *Lactococcus* and *Romboutsia* at the genus level (Fig. 9f). However, the AKG diet exerted adverse effects on several microbiota like *Butyricicoccus*, *Lachnospiraceae_NK4A136_group*, *Roseburia*, and *Lactococcus* in the AAV-*h*α-Syn and AAV-GFP groups (Fig. 9f). We then performed correlation analysis between gut microbiota and microbial metabolites which were altered by the AKG diet in mice injected with AAV-*h*α-Syn (Fig. 9g, Supplementary Fig. 17a). Here, we show the top hit results between the *Lachnospiraceae_NK4A136_group*, *Lactococcus,* and microbial metabolites. The *Lachnospiraceae_NK4A136_group* was negatively correlated with 11-dehydro-thromboxane B2, prostaglandin G2, leukotriene D4, leukotriene E4, and positively correlated with prostaglandin A2 and 6-keto-prostaglandin F1a (Fig. 9h–m), where *Lactococcus* had a contrary correlation with the above-mentioned microbial metabolites (Supplementary Fig. 17b–g). Thus, we revealed gut microbiota and metabolome alterations due to ingestion of the AKG diet in AAV-*h*α-Syn mice, which may communicate with nigral metabolism through the gut-brain axis.

Dietary intake of AKG ameliorates movement disorder, α-synuclein pathology and DA neuron degeneration in transgenic A53T α-Syn mice

Since we have observed the protective effects of AKG in the AAV-*h*α-Syn mice, we want to exclude these effects are due to AKG suppressing the efficacy of AAV transduction, in addition, we are also eager to verify our finding in the transgenic mice model, thus we utilized the A53T α-Syn mice. Here, we found A53T α-Syn mice behave obvious parkinsonian phenotypes, motor dysfunction (impaired travelled distance and movement speed in the open field test, increased pole-climbing time, and decreased duration in the rotarod and holding time score), enhanced α-synuclein pathology and nigrostriatal DA neuron degeneration (Fig. 10a–l). Dietary intake of AKG for 12 weeks significantly improved the total travelled distance, movement speed, number of entries to the center, and time spent in the center in the open field test of A53T α-Syn mice (Fig. 10a–f). Moreover, the AKG diet also decreased pole-climbing time and increased motor coordination and grip strength in A53T α-Syn mice (Fig. 10g–i). Furthermore, the AKG diet significantly reduced nigral and striatal α-synuclein pathology in A53T α-Syn mice (Fig. 10j and k), and also promoted striatal and nigral DA neuron activity in A53T α-Syn mice (Fig. 10l–n).

The AKG diet increased nigral and serum AKG levels in A53T α-Syn mice (Fig. 11a and b). Besides, the AKG diet increased the endpoint voxels and branch length, and decreased the cellular volume of Iba1 + cells, suggesting it suppressed microglial activation in A53T α-Syn mice (Fig. 11c). AKG also increased nigral and striatal synapsin, PSD-95 expression, and striatal syntaxin expression in A53T α-Syn mice (Fig. 11d and e). Consistently, the AKG diet promoted the number of nigral synaptic vesicles and VMAT2-positive neurons in A53T α-Syn mice (Fig. 11f and g). Neither vGAT or vGLUT2-positive cells were changed in WT, AKG, A53T α-Syn or A53T α-Syn + AKG mice (Supplementary Fig. 18a and b). Taken together, the results show that the AKG diet improved motor dysfunction, α-synuclein pathology, and decreased DA neuron death in A53T α-Syn mice.

Discussion

During the TCA cycle, AKG is converted from isocitrate and glutamate to succinyl-CoA. Additionally, AKG is also a significant source of cellular adenosine triphosphate [42]. Emerging evidence supports AKG as a new anti-aging agent [11–15]. Although AKG was found to modulate mTOR signaling to extend the lifespan of *C. elegans* and *Drosophila* [11, 12], this cascade was not found in mice [15]. Moreover, dietary AKG was found to hinder chronic inflammation by producing anti-inflammatory IL-10 [15]. Here, we report that an AKG diet improved movement disorder, α-synuclein pathology, and impaired DA synapses in PD mouse models.

By virtue of RNA-seq, we reveal that AKG promotes the complement-related pathways. Especially, we found the reduced expression of microglial phosphorylated α-synuclein, alongside the increased expression of C1q in the microglia. As the initiating protein of the classical complement cascade, C1q is thought to be neurotoxic and contributes to neuronal death and synapse loss in neurodegenerative diseases and neurological disorders [34, 43, 44]. However, C1q has also been shown to be neuroprotective by preventing β-amyloid-induced neurotoxicity and enhancing the phagocytosis of microglia [35–37, 45]. Inspired by this idea, we hypothesized that C1q may be responsible for the clearance of phosphorylated α-synuclein upon AKG treatment. Through transcriptomic analysis and validation, we

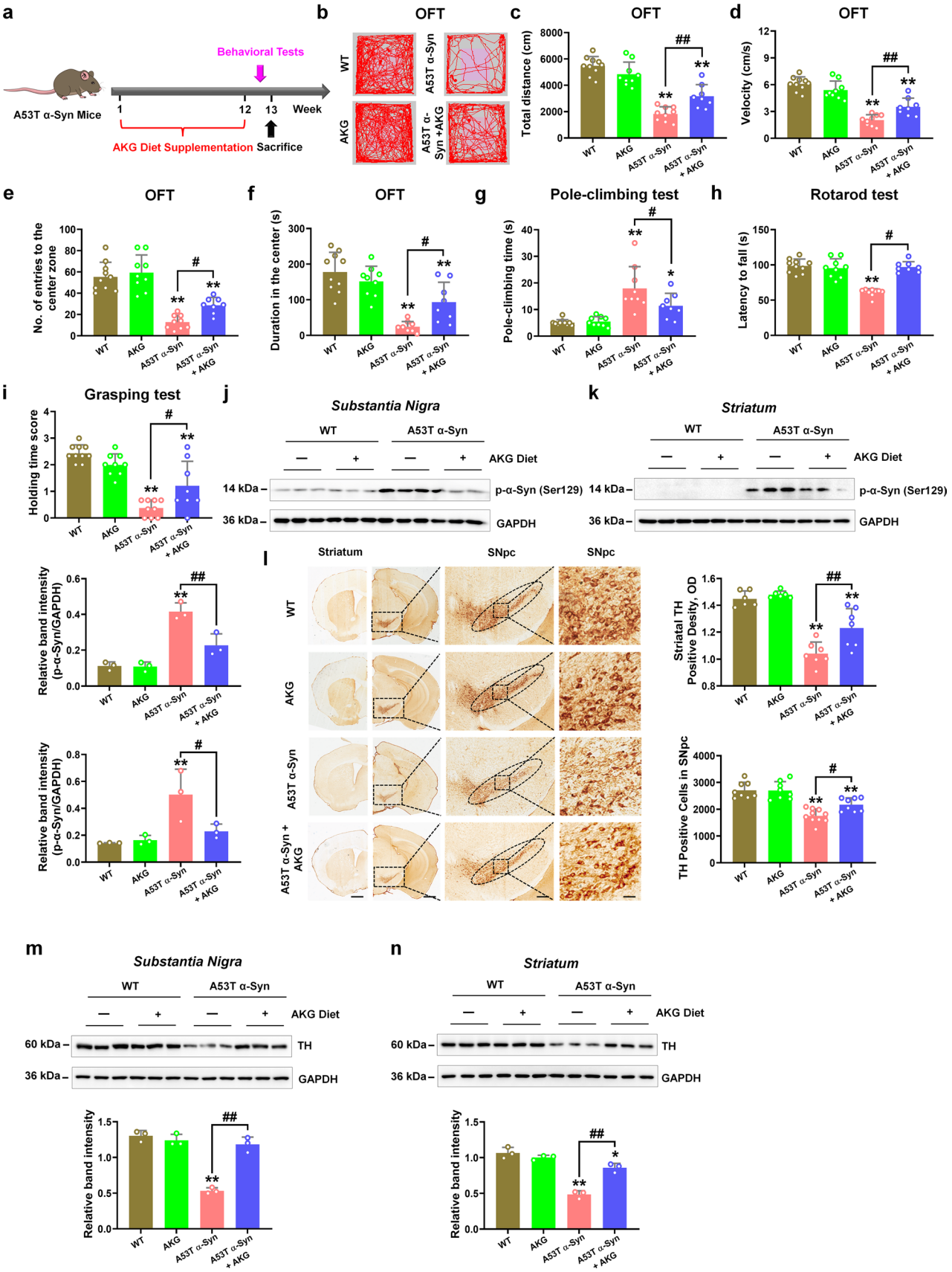
a
Behavioral Tests
A53T α-Syn Mice
1
12
13
Week
AKG Diet Supplementation
Sacrifice
b
OFT
WT
A53T α-Syn
AKG
A53T α-Syn +AKG
c
OFT
Total distance (cm)
d
OFT
Velocity (cm/s)
e
OFT
No. of entries to the center zone
f
OFT
Duration in the center (s)
g
Pole-climbing test
Pole-climbing time (s)
h
Rotarod test
Latency to fall (s)
i
Grasping test
Holding time score
j
Substantia Nigra
WT
A53T α-Syn
AKG Diet
14 kDa
p-α-Syn (Ser129)
36 kDa
GAPDH
k
Striatum
WT
A53T α-Syn
AKG Diet
14 kDa
p-α-Syn (Ser129)
36 kDa
GAPDH
Relative band intensity (p-α-Syn/GAPDH)
Relative band intensity (p-α-Syn/GAPDH)
l
Striatum
SNpc
SNpc
WT
AKG
A53T α-Syn
A53T α-Syn + AKG
Striatal TH Positive Desity, OD
TH Positive Cells in SNpc
m
Substantia Nigra
WT
A53T α-Syn
AKG Diet
60 kDa
TH
36 kDa
GAPDH
Relative band intensity
n
Striatum
WT
A53T α-Syn
AKG Diet
60 kDa
TH
36 kDa
GAPDH
Relative band intensity

◂**Fig. 10** The AKG diet attenuates the parkinsonian phenotype in transgenic A53T α-Syn mice. **a** Experimental design for AKG diet administration in A53T α-Syn mice. **b**–**f** Representative traces, total travelled distance, movement speed, the number of entries to the center zone, and time spent in the center zone in the open field test. **g** The pole-climbing test was used to examine bradykinesia in the mice. **h** The rotarod test was used to examine the motor coordination of the mice. **i** The grasping test was used to examine the grip strength of the mice. n = 10, 9, 9 and 8 for WT, AKG, A53T α-Syn and A53T α-Syn + AKG, respectively. **j** and **k** Representative blots and quantification showing the expression of phosphorylated α-synuclein (Ser129) in the SN and striatum. n = 3 per group. **l** Immunohistochemistry staining and quantification of TH-positive cells in SNpc and TH-positive density in the striatum. Scale bars, 1 mm for striatum, 800 μm for SNpc. Magnified images of TH-positive cells in the SNpc are shown in the right column of the panel (**l**). n = 6–10. Scale bars, 100 μm. **m** and **n** Representative blots and quantification showing TH expression in the SN and striatum. n = 3 per group. Results are expressed as the mean ± SEM. $^{**}p < 0.01$, $^{*}p < 0.05$ vs. WT; $^{\#\#}p < 0.01$, $^{\#}p < 0.05$ vs. A53T α-Syn. Statistical significance was determined using one-way ANOVA and Tukey's test for post hoc comparisons

found that the AKG diet significantly increased the mRNA expression of *C1qa*, and we also noted that the reduced phosphorylated α-synuclein within microglia in the SN of AAV-*h*α-Syn mice. Since microglia are the main source of C1q [46], our in vivo and in vitro data suggest that the induced microglial autophagy mediated by C1q underlies this effect. Our results also indicated AKG treatment could reduce the expression of phosphorylated α-synuclein in A53T α-Syn Tg mice, which could exclude the effect is mediated by AKG suppressing the efficacy of AAV transduction. Collectively, we claim that C1q-mediated autophagy underlies AKG reducing the levels of phosphorylated α-synuclein in the α-synucleinopathy models of PD.

In this study, AAV-*h*α-Syn caused a reduction in the number of synaptic vesicles, which is pathologically relevant to α-synuclein burden. Importantly, we found reduced VMAT2 (responsible for dopamine release)-positive cells, rather than vGAT (inhibitory neurons) or vGLUT2 (excitatory neurons)-positive cells in the SN of AAV-*h*α-Syn-injected and transgenic A53T α-Syn mice. These results suggest that AAV-*h*α-Syn may reduce VMAT2-positive synaptic vesicles, which is related to the DA neuron degeneration we observed. These results were consistent with previous study [26]. Since α-synuclein is a pre-synaptic terminal protein under physiological conditions, increased α-synuclein expression was reported to reduce neurotransmitter release by hindering synaptic vesicle reclustering after endocytosis [47]. Besides, pathological α-synuclein could damage cellular vesicles by permeabilizing cholesterol-containing vesicular membranes and inducing DA leak from vesicles into the cytosol [48]. Additionally, the effects of α-synuclein overexpression on synaptic vesicles may be resulted from it induced pro-inflammatory response and oxidative stress [38, 49]. In this study, we found AKG administration increased the number of synaptic vesicles in AAV-*h*α-Syn and A53T α-Syn mice. We conclude this neuroprotection was due to AKG's autophagy induction and anti-inflammatory effects. Our data suggest a loss of VMAT2-ir axon terminals in the SNc but could not tell the neurochemical identity of axon terminals with higher number of SVs, we may need to clarify the synaptic vesicle number and clustering related to AAV-*h*α-Syn damage in the future.

Another interesting finding from our study was that the AKG diet increased nigral DHA levels in a PD model. DHA has been proved to be beneficial for the treatment of depression, schizophrenia, and aging-related diseases such as PD and AD [50–53]. Previously, DHA intake was found to extend the longevity of mice overexpressing human α-synuclein, possibly through regulating enteric DA neurons, while DHA exerted no obvious effects on motor impairment, the nigral DA system, and α-synuclein levels [54, 55]. However, other studies have provided evidence that DHA may improve movement disorders and dopamine synthesis in 6-OHDA- and rotenone-induced rodent PD models via regulating protein kinase activity and suppressing inflammation and oxidative stress [32, 33, 56, 57]. Here, our metabolomic analysis revealed that the AKG diet increased nigral DHA concentration, and DHA ameliorated motor dysfunction and reduced α-synuclein pathology in a PD mouse model. DHA may share the similar neuroprotective mechanisms with AKG.

How ingestion of the AKG diet produced nigral DHA? We explored the gut-brain-axis mechanism of dietary AKG intake, and the differential microbial metabolites were enriched in "Alpha Linolenic acid metabolism", "Linoleic acid Metabolism", and "AA metabolism", suggesting the AKG diet modulates enteric omega-6 and omega-3 PUFA metabolism. PUFAs contain two main types: omega-6 fatty acids with its 18C precursor linoleic acid, and the omega-3 fatty acids, with its 18C precursor alpha-linolenic acid. Omega-6 linoleic acid is metabolized to arachidonic acid (AA) and omega-3 alpha-linolenic acid is metabolized to DHA and eicosapentaenoic acid (EPA) [58]. DHA was previously found to modulate TCA cycle homeostasis [59, 60]. Because AKG is a key intermediate product during the TCA cycle, we conclude that energy metabolism may be the link between AKG and DHA. In addition, we noted that AKG significantly decreased the abundance of *Roseburia* in AAV-*h*α-Syn mice. *Roseburia* is a prominent gut-associated butyrate-producing bacteria [61, 62], and sodium butyrate was found to interact with DHA to increase omega-3 fatty acid level and induce apoptosis in cancer cells [63, 64]. Notably, sodium butyrate was reported to exacerbate PD pathology by aggravating colonic inflammation [65]. Thus, we hypothesize that AKG-increased nigral DHA levels may be compensatory to the aberrant gut microbiota and microbial metabolites.

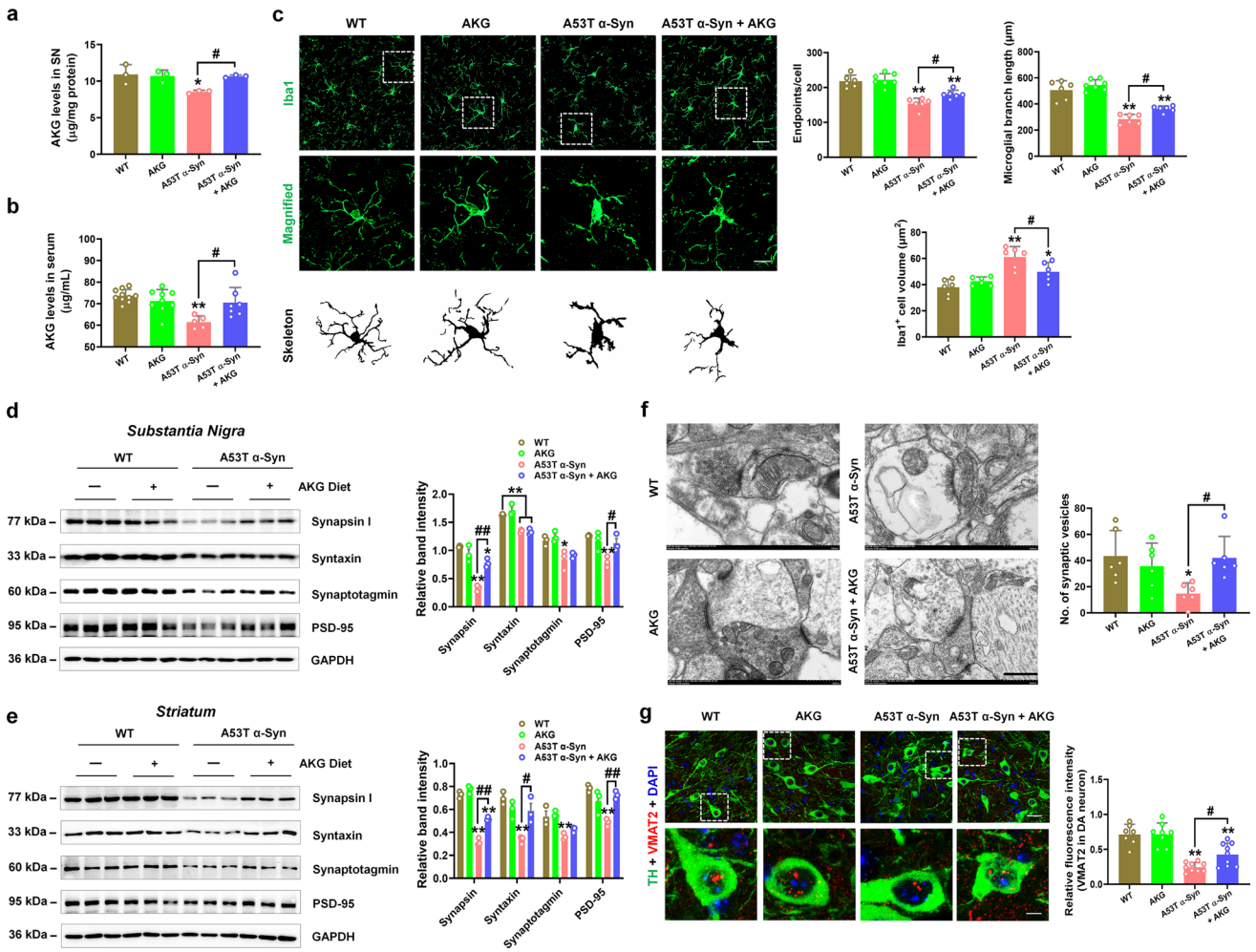

Fig. 11 The AKG diet suppresses the pro-inflammatory response and rescues impaired DA synapses in A53T α-Syn mice. **a** and **b** AKG levels in the SN and serum were determined by ELISA. n = 3 for SN, n = 5–10 for serum. **c** Immunofluorescence staining and quantification of endpoint voxels, branch length, and volume of Iba1-positive cells in the SN of WT, AKG, A53T α-Syn, and A53T α-Syn + AKG groups. Scale bars, 40 μm. Magnified images are shown in the middle row, and skeletal diagrams of Iba1-positive cells are shown in the bottom row. Scale bars, 12 μm. n = 6–7. **d** and **e** Representative blots and quantification showing the expression of Synapsin, Syntaxin, Synaptotagmin, and PSD-95 in the SN and striatum. n = 3 per group. **f** The representative images and quantitative analysis of ultrastructural synaptic vesicles in the SN. n = 6 per group. Scale bars, 500 μm. **g** Immunofluorescence staining and quantification of VMAT2 within TH-positive cells in the SN of WT, AKG, A53T α-Syn, and A53T α-Syn + AKG groups. Scale bars, 40 μm. Magnified images are shown in the bottom row. Scale bars, 10 μm. n = 7–9. Results are expressed as the mean ± SEM. $^{**}p < 0.01$, $^{*}p < 0.05$ vs. WT; $^{\#\#}p < 0.01$, $^{\#}p < 0.05$ vs. A53T α-Syn. Statistical significance was determined using one-way ANOVA and Tukey's test for post hoc comparisons

Our study also reveals the gut-brain-axis mechanism of AKG and DHA in attenuating the pro-inflammatory response in a PD model. Previous study reveal that lack of microbiota diversity results in defects in microglia, and microbiota-derived short-chain fatty acids (SCFAs) could modulate the microglia homeostasis [66]. The "anti-inflammatory" SCFAs, butyrate-producing bacteria *Blautia*, *Coprococcus*, and *Roseburia* were found to be reduced in the fecal samples of PD patients, while *Ralstonia* was significantly increased in mucosa of PD patients [67]. Mechanistically, butyrate could inhibit TLR4/MyD88/NF-κB pathway in the colon and striatum, and suppress the production of proinflammatory cytokines [68, 69]. Nigral α-synuclein overexpression induces significant neuronal loss in the ileal submucosal plexus and increases fecal bile acid composition in the AAV-α-synuclein-injected PD rat model [70], suggesting nigral α-synuclein pathology actually affects the enteric nervous system and gut microbial metabolism. In addition, SCFAs are also responsible for the microglia activation and α-synuclein aggregation in α-synuclein-overexpressing mice [40]. In this study, the AKG diet increased enteric 11-dehydro-thromboxane B2, prostaglandin G2, leukotriene D4,

and leukotriene E4 in AAV-*h*α-Syn mice. These metabolites are related to AA metabolism and pro-inflammatory reactions. For example, 11-Dehydro-thromboxane B2 is a stable metabolite of thromboxane A2, which is a cyclooxygenase product of AA [71]; prostaglandin G2 is converted from AA via cyclooxygenase [72]; leukotriene D4 and leukotriene E4 are also produced from AA [73]. In addition, the AKG diet decreased enteric prostaglandin A2 and 6-keto-prostaglandin F1a. Prostaglandin A2 has been shown to suppress LPS-induced inflammatory signaling by inhibiting the NF-κB pathway [74]. In addition, 6-Keto-prostaglandin F1 is a stable hydrolysis product of prostacyclin (prostaglandin I2, PGI2), which is proved to be an important inflammatory mediator [75]. Considering both AKG and DHA suppress the pro-inflammatory response in the brain, we conclude that the AKG diet-regulated enteric inflammatory state may be a compensatory effect of the α-synuclein burden in the brain and this is potentially related to platelet activity, as most altered microbial metabolites are linked to platelets. We also identified several gut microbes which may be correlated to modulation of microbial metabolites. *Lachnospiraceae_NK4A136_group* was negatively correlated with 11-dehydro-thromboxane B2, prostaglandin G2, leukotriene D4, leukotriene E4 and positively correlated with prostaglandin A2 and 6-keto-prostaglandin F1a. Previously, *Lachnospiraceae_NK4A136_group* was found to be responsible for spermidine-enhanced gut barrier function and its protection against obesity [76], it was also was negatively correlated with oxidative stress and inflammation in the gut [77, 78]. This finding further confirms our hypothesis that AKG modulated the gut microbiota and microbial metabolism to be resistant to nigral α-synuclein burden-induced intestinal chaos. Moreover, modulating PUFA metabolism in the gut-brain axis may underlie the benefits of AKG in PD mice.

In the current study, the AKG diet was given for at least 3 months to efficiently clear the α-synuclein pathology. We conclude that long-term dietary AKG supplementation may be beneficial for PD treatment, however, potential side effects require further examination. Moreover, there are few studies indicating the potential beneficial effects of AKG supplementation in humans. AKG is usually used in pure form or combined with other elements (such as calcium, arginine, ornithine, or sodium). Some studies report that ornithine AKG (O-AKG) improved wound healing in severe burn patients [79, 80]. Recently, Rejuvant® (an AKG-based formulation) was revealed to decrease the biological aging of humans by eight years, as measured by DNA methylation, suggesting its potential anti-aging role [81]. Nevertheless, clinical trials using AKG-based formulations in PD patients is urgent. Due to its metabolic properties and pharmacokinetics, 80% of dietary AKG is rapidly removed from the bloodstream [82]. The daily dose of AKG ranges from 3.6–30 g in humans [79, 83–85], and our study indicates that dietary Ca-AKG (2%) could induce autophagy and clear misfolded α-synuclein in the mouse model. The dietary dose used in PD patients still needs further clinical investigation.

In summary, we show that dietary intake of AKG induced microglia to phagocytose and degrade α-synuclein via upregulating C1q signaling and suppressed pro-inflammatory reactions in AAV-*h*α-Syn mice and A53T α-Syn mice. We also suggest that the AKG diet increased nigral DHA levels in the PD mice model. Additionally, we determined the gut-brain axis mechanism behind the benefits of the AKG diet in α-synucleinopathy mouse models. Taken together, our findings propose that dietary intake of AKG is a promising therapeutic approach for PD.

Supplementary Information The online version contains supplementary material available at https://doi.org/10.1007/s00018-023-04807-7.

Author contributions YLZ designed the research. WLZ and MRZ performed the Western blotting. LYD and RFM carried out the immunostaining assays. JWG and SHZ injected the AAVs and performed the behavioral tests. HXM prepared and provided the human PFF. YLZ, WLZ, LYD and MRZ analyzed the data. YLZ wrote the manuscript. PYX and HXX discussed the manuscript. All authors read and commented on it.

Funding This work was supported by the National Natural Science Foundation of China (No. 82174468 to Y.L.Z., No. 81870856, 81870992, 82071416 to P.Y.X., No. 82101325 to W.L.Z.), the Science and Technology Planning Project of Guangzhou (No. 201904010238 to Y.L.Z.), Guangzhou Medical University Discipline Construction Funds (Basic Medicine, No. JCXKJS2022A09 to Y.L.Z.), Central government guiding local science and technology development projects (No. ZYYD2022C17 to P.Y.X.), Key Research and Development Program of Guangzhou (No. 2023B03J0631 to P.Y.X.), Municipal University (Faculty) joint funding project (No. 202102010010 to P.Y.X.), Guangdong Basic and Applied Basic Research Foundation (No. 2022B1515230004 to P.Y.X.), and the China Postdoctoral Science Foundation (No. 2021M700951 to W.L.Z.).

Data availability All data needed to evaluate the conclusions in the paper are present in the paper and/or the supplementary files, and the RNA-seq data can be publicly found at the Gene Expression Omnibus database under accession number GSE214446. Requests for any materials in this study should be directed to Yunlong Zhang and obtained through an MTA.

Declarations

Conflict of interest The authors have no relevant financial or non-financial interests to disclose.

Ethical approval The animal study was approved by the guidelines of the Institutional Animal Care and Use Committee of the Guangzhou Medical University and in line with the National Institutes of Health guidelines on the care and use of animals (NIH Publications No. 8023, revised 1978).

References

1. Kalia LV, Lang AE (2015) Parkinson's disease. Lancet 386(9996):896–912
2. Samii A, Nutt JG, Ransom BR (2004) Parkinson's disease. Lancet 363(9423):1783–1793
3. Armstrong MJ, Okun MS (2020) Diagnosis and treatment of Parkinson disease: a review. JAMA 323(6):548–560
4. Fox SH, Lang AE (2008) Levodopa-related motor complications–phenomenology. Mov Disord 23(Suppl 3):S509-514
5. Petzinger GM, Fisher BE, McEwen S, Beeler JA, Walsh JP, Jakowec MW (2013) Exercise-enhanced neuroplasticity targeting motor and cognitive circuitry in Parkinson's disease. Lancet Neurol 12(7):716–726
6. Domenighetti C, Sugier PE, Ashok Kumar Sreelatha A, Schulte C, Grover S, Mohamed O et al (2022) Dairy intake and Parkinson's disease: a Mendelian randomization study. Mov Disord 37(4):857–864
7. Tan AH, Lim SY, Chong KK, Manap MAAA, Hor JW, Lim JL et al (2021) Probiotics for constipation in Parkinson disease: a randomized placebo-controlled study. Neurology 96(5):e772–e782
8. Goya ME, Xue F, Sampedro-Torres-Quevedo C, Arnaouteli S, Riquelme-Dominguez L, Romanowski A et al (2020) Probiotic bacillus subtilis protects against alpha-synuclein aggregation in *C. elegans*. Cell Rep 30(2):367-380 e367
9. Maraki MI, Yannakoulia M, Stamelou M, Stefanis L, Xiromerisiou G, Kosmidis MH et al (2019) Mediterranean diet adherence is related to reduced probability of prodromal Parkinson's disease. Mov Disord 34(1):48–57
10. Phillips MCL, Murtagh DKJ, Gilbertson LJ, Asztely FJS, Lynch CDP (2018) Low-fat versus ketogenic diet in Parkinson's disease: a pilot randomized controlled trial. Mov Disord 33(8):1306–1314
11. Chin RM, Fu X, Pai MY, Vergnes L, Hwang H, Deng G et al (2014) The metabolite alpha-ketoglutarate extends lifespan by inhibiting ATP synthase and TOR. Nature 510(7505):397–401
12. Su Y, Wang T, Wu N, Li D, Fan X, Xu Z et al (2019) Alpha-ketoglutarate extends drosophila lifespan by inhibiting mTOR and activating AMPK. Aging (Albany NY) 11(12):4183–4197
13. Burdyliuk N, Bayliak M (2017) Effects of long-term cultivation on medium with alpha-ketoglutarate supplementation on metabolic processes of *Saccharomyces cerevisiae*. J Aging Res 2017:8754879
14. Zhang Z, He C, Gao Y, Zhang L, Song Y, Zhu T et al (2021) Alpha-ketoglutarate delays age-related fertility decline in mammals. Aging Cell 20(2):e13291
15. Asadi Shahmirzadi A, Edgar D, Liao CY, Hsu YM, Lucanic M, Asadi Shahmirzadi A et al (2020) Alpha-ketoglutarate, an endogenous metabolite, extends lifespan and compresses morbidity in aging mice. Cell Metab 32(3):447-456 e446
16. An D, Zeng Q, Zhang P, Ma Z, Zhang H, Liu Z et al (2021) Alpha-ketoglutarate ameliorates pressure overload-induced chronic cardiac dysfunction in mice. Redox Biol 46:102088
17. Wang Y, Deng P, Liu Y, Wu Y, Chen Y, Guo Y et al (2020) Alpha-ketoglutarate ameliorates age-related osteoporosis via regulating histone methylations. Nat Commun 11(1):5596
18. Salminen A, Kauppinen A, Hiltunen M, Kaarniranta K (2014) Krebs cycle intermediates regulate DNA and histone methylation: epigenetic impact on the aging process. Ageing Res Rev 16:45–65
19. Volpicelli-Daley LA, Luk KC, Lee VM (2014) Addition of exogenous alpha-synuclein preformed fibrils to primary neuronal cultures to seed recruitment of endogenous alpha-synuclein to lewy body and lewy neurite-like aggregates. Nat Protoc 9(9):2135–2146
20. Zhang W, Ding L, Chen H, Zhang M, Ma R, Zheng S et al (2023) Cntnap4 partial deficiency exacerbates alpha-synuclein pathology through astrocyte-microglia c3–c3ar pathway. Cell Death Dis 14(4):285
21. Polinski NK, Volpicelli-Daley LA, Sortwell CE, Luk KC, Cremades N, Gottler LM et al (2018) Best practices for generating and using alpha-synuclein pre-formed fibrils to model Parkinson's disease in rodents. J Parkinsons Dis 8(2):303–322
22. Zhou C, Zhong W, Zhou J, Sheng F, Fang Z, Wei Y et al (2012) Monitoring autophagic flux by an improved tandem fluorescent-tagged lc3 (mtagrfp-mwasabi-lc3) reveals that high-dose rapamycin impairs autophagic flux in cancer cells. Autophagy 8(8):1215–1226
23. Giasson BI, Duda JE, Quinn SM, Zhang B, Trojanowski JQ, Lee VM (2002) Neuronal alpha-synucleinopathy with severe movement disorder in mice expressing a53t human alpha-synuclein. Neuron 34(4):521–533
24. Liu JH, Wang Q, You QL, Li ZL, Hu NY, Wang Y et al (2020) Acute EPA-induced learning and memory impairment in mice is prevented by DHA. Nat Commun 11(1):5465
25. Gong J, Zhang W, Ding L, Zhang M, Zheng S, Ma R et al (2021) 4,4'-dimethoxychalcone regulates redox homeostasis by targeting riboflavin metabolism in Parkinson's disease therapy. Free Radic Biol Med 174:40–56
26. Faustini G, Longhena F, Varanita T, Bubacco L, Pizzi M, Missale C et al (2018) Synapsin III deficiency hampers alpha-synuclein aggregation, striatal synaptic damage and nigral cell loss in an AAV-based mouse model of Parkinson's disease. Acta Neuropathol 136(4):621–639
27. Zhang W, Chen H, Ding L, Gong J, Zhang M, Guo W et al (2021) Trojan horse delivery of 4,4'-dimethoxychalcone for parkinsonian neuroprotection. Adv Sci (Weinh) 8(9):2004555
28. Zhang W, Zhou M, Lu W, Gong J, Gao F, Li Y et al (2020) Cntnap4 deficiency in dopaminergic neurons initiates parkinsonian phenotypes. Theranostics 10(7):3000–3021
29. Zhang W, Huang J, Gao F, You Q, Ding L, Gong J et al (2022) *Lactobacillus reuteri* normalizes altered fear memory in male *Cntnap4* knockout mice. EBioMedicine 86:104323
30. Zhang M, Chen H, Zhang W, Liu Y, Ding L, Gong J et al (2023) Biomimetic remodeling of microglial riboflavin metabolism ameliorates cognitive impairment by modulating neuroinflammation. Adv Sci (Weinh). https://doi.org/10.1002/advs.202300180
31. Chang PK, Khatchadourian A, McKinney RA, Maysinger D (2015) Docosahexaenoic acid (DHA): a modulator of microglia activity and dendritic spine morphology. J Neuroinflammation 12:34
32. Chitre NM, Wood BJ, Ray A, Moniri NH, Murnane KS (2020) Docosahexaenoic acid protects motor function and increases dopamine synthesis in a rat model of Parkinson's disease via mechanisms associated with increased protein kinase activity in the striatum. Neuropharmacology 167:107976
33. Serrano-Garcia N, Fernandez-Valverde F, Luis-Garcia ER, Granados-Rojas L, Juarez-Zepeda TE, Orozco-Suarez SA et al (2018) Docosahexaenoic acid protection in a rotenone induced Parkinson's model: prevention of tubulin and synaptophysin loss, but no association with mitochondrial function. Neurochem Int 121:26–37
34. Holden SS, Grandi FC, Aboubakr O, Higashikubo B, Cho FS, Chang AH et al (2021) Complement factor c1q mediates sleep spindle loss and epileptic spikes after mild brain injury. Science 373(6560):eabj2685
35. Webster SD, Galvan MD, Ferran E, Garzon-Rodriguez W, Glabe CG, Tenner AJ (2001) Antibody-mediated phagocytosis of the amyloid beta-peptide in microglia is differentially modulated by c1q. J Immunol 166(12):7496–7503
36. Webster SD, Park M, Fonseca MI, Tenner AJ (2000) Structural and functional evidence for microglial expression of C1qr(p),

the c1q receptor that enhances phagocytosis. J Leukoc Biol 67(1):109–116
37. Webster SD, Yang AJ, Margol L, Garzon-Rodriguez W, Glabe CG, Tenner AJ (2000) Complement component C1q modulates the phagocytosis of abeta by microglia. Exp Neurol 161(1):127–138
38. Choi I, Zhang Y, Seegobin SP, Pruvost M, Wang Q, Purtell K et al (2020) Microglia clear neuron-released alpha-synuclein via selective autophagy and prevent neurodegeneration. Nat Commun 11(1):1386
39. Cao S, Theodore S, Standaert DG (2010) Fcgamma receptors are required for nf-kappab signaling, microglial activation and dopaminergic neurodegeneration in an AAV-synuclein mouse model of Parkinson's disease. Mol Neurodegener 5:42
40. Sampson TR, Debelius JW, Thron T, Janssen S, Shastri GG, Ilhan ZE et al (2016) Gut microbiota regulate motor deficits and neuroinflammation in a model of Parkinson's disease. Cell 167(6):1469-1480 e1412
41. Sampson TR, Challis C, Jain N, Moiseyenko A, Ladinsky MS, Shastri GG et al (2020) A gut bacterial amyloid promotes alpha-synuclein aggregation and motor impairment in mice. Elife. https://doi.org/10.7554/eLife.53111
42. He L, Xu Z, Yao K, Wu G, Yin Y, Nyachoti CM et al (2015) The physiological basis and nutritional function of alpha-ketoglutarate. Curr Protein Pept Sci 16(7):576–581
43. Hong S, Beja-Glasser VF, Nfonoyim BM, Frouin A, Li S, Ramakrishnan S et al (2016) Complement and microglia mediate early synapse loss in Alzheimer mouse models. Science 352(6286):712–716
44. Absinta M, Maric D, Gharagozloo M, Garton T, Smith MD, Jin J et al (2021) A lymphocyte-microglia-astrocyte axis in chronic active multiple sclerosis. Nature 597(7878):709–714
45. Pisalyaput K, Tenner AJ (2008) Complement component C1q inhibits beta-amyloid- and serum amyloid p-induced neurotoxicity via caspase- and calpain-independent mechanisms. J Neurochem 104(3):696–707
46. Fonseca MI, Chu SH, Hernandez MX, Fang MJ, Modarresi L, Selvan P et al (2017) Cell-specific deletion of C1qa identifies microglia as the dominant source of C1q in mouse brain. J Neuroinflammation 14(1):48
47. Nemani VM, Lu W, Berge V, Nakamura K, Onoa B, Lee MK et al (2010) Increased expression of alpha-synuclein reduces neurotransmitter release by inhibiting synaptic vesicle reclustering after endocytosis. Neuron 65(1):66–79
48. Plotegher N, Berti G, Ferrari E, Tessari I, Zanetti M, Lunelli L et al (2017) Dopal derived alpha-synuclein oligomers impair synaptic vesicles physiological function. Sci Rep 7:40699
49. Chen MK, Kuwabara H, Zhou Y, Adams RJ, Brasic JR, McGlothan JL et al (2008) VMAT2 and dopamine neuron loss in a primate model of Parkinson's disease. J Neurochem 105(1):78–90
50. Makrides M, Gibson RA, McPhee AJ, Yelland L, Quinlivan J, Ryan P et al (2010) Effect of DHA supplementation during pregnancy on maternal depression and neurodevelopment of young children: a randomized controlled trial. JAMA 304(15):1675–1683
51. Borsini A, Nicolaou A, Camacho-Munoz D, Kendall AC, Di Benedetto MG, Giacobbe J et al (2021) Omega-3 polyunsaturated fatty acids protect against inflammation through production of LOX and CYP450 lipid mediators: relevance for major depression and for human hippocampal neurogenesis. Mol Psychiatry 26(11):6773–6788
52. Patrick RP (2019) Role of phosphatidylcholine-DHA in preventing APOE4-associated Alzheimer's disease. FASEB J 33(2):1554–1564
53. Qiao Y, Mei Y, Han H, Liu F, Yang XM, Shao Y et al (2018) Effects of omega-3 in the treatment of violent schizophrenia patients. Schizophr Res 195:283–285
54. Coulombe K, Kerdiles O, Tremblay C, Emond V, Lebel M, Boulianne AS et al (2018) Impact of DHA intake in a mouse model of synucleinopathy. Exp Neurol 301(Pt A):39–49
55. Lamontagne-Proulx J, Coulombe K, Dahhani F, Cote M, Guyaz C, Tremblay C et al (2021) Effect of docosahexaenoic acid (DHA) at the enteric level in a synucleinopathy mouse model. Nutrients. https://doi.org/10.3390/nu13124218
56. Coulombe K, Saint-Pierre M, Cisbani G, St-Amour I, Gibrat C, Giguere-Rancourt A et al (2016) Partial neurorescue effects of dha following a 6-ohda lesion of the mouse dopaminergic system. J Nutr Biochem 30:133–142
57. Hernando S, Requejo C, Herran E, Ruiz-Ortega JA, Morera-Herreras T, Lafuente JV et al (2019) Beneficial effects of n-3 polyunsaturated fatty acids administration in a partial lesion model of Parkinson's disease: the role of glia and NRf2 regulation. Neurobiol Dis 121:252–262
58. Bradbury J (2011) Docosahexaenoic acid (DHA): an ancient nutrient for the modern human brain. Nutrients 3(5):529–554
59. Liu R, Chen L, Wang Z, Zheng X, Hou Z, Zhao D et al (2021) Omega-3 polyunsaturated fatty acids prevent obesity by improving tricarboxylic acid cycle homeostasis. J Nutr Biochem 88:108503
60. Bahety P, Tan YM, Hong Y, Zhang L, Chan EC, Ee PL (2014) Metabotyping of docosahexaenoic acid—treated Alzheimer's disease cell model. PLoS ONE 9(2):e90123
61. Machiels K, Joossens M, Sabino J, De Preter V, Arijs I, Eeckhaut V et al (2014) A decrease of the butyrate-producing species *Roseburia hominis* and *Faecalibacterium prausnitzii* defines dysbiosis in patients with ulcerative colitis. Gut 63(8):1275–1283
62. Kasahara K, Krautkramer KA, Org E, Romano KA, Kerby RL, Vivas EI et al (2018) Interactions between *Roseburia intestinalis* and diet modulate atherogenesis in a murine model. Nat Microbiol 3(12):1461–1471
63. Tylichova Z, Slavik J, Ciganek M, Ovesna P, Krcmar P, Strakova N et al (2018) Butyrate and docosahexaenoic acid interact in alterations of specific lipid classes in differentiating colon cancer cells. J Cell Biochem 119(6):4664–4679
64. Kolar S, Barhoumi R, Jones CK, Wesley J, Lupton JR, Fan YY et al (2011) Interactive effects of fatty acid and butyrate-induced mitochondrial ca(2)(+) loading and apoptosis in colonocytes. Cancer 117(23):5294–5303
65. Qiao CM, Sun MF, Jia XB, Li Y, Zhang BP, Zhao LP et al (2020) Sodium butyrate exacerbates Parkinson's disease by aggravating neuroinflammation and colonic inflammation in MPTP-induced mice model. Neurochem Res 45(9):2128–2142
66. Erny D, Hrabe de Angelis AL, Jaitin D, Wieghofer P, Staszewski O, David E et al (2015) Host microbiota constantly control maturation and function of microglia in the CNS. Nat Neurosci 18(7):965–977
67. Keshavarzian A, Green SJ, Engen PA, Voigt RM, Naqib A, Forsyth CB et al (2015) Colonic bacterial composition in Parkinson's disease. Mov Disord 30(10):1351–1360
68. Segain JP, Raingeard de la Bletiere D, Bourreille A, Leray V, Gervois N, Rosales C et al (2000) Butyrate inhibits inflammatory responses through nfkappab inhibition: implications for Crohn's disease. Gut 47(3):397–403
69. Guo TT, Zhang Z, Sun Y, Zhu RY, Wang FX, Ma LJ et al (2023) Neuroprotective effects of sodium butyrate by restoring gut microbiota and inhibiting TLR4 signaling in mice with MPTP-induced Parkinson's disease. Nutrients. https://doi.org/10.3390/nu15040930
70. O'Donovan SM, Crowley EK, Brown JR, O'Sullivan O, O'Leary OF, Timmons S et al (2020) Nigral overexpression of alpha-synuclein in a rat Parkinson's disease model indicates alterations in the enteric nervous system and the gut microbiome. Neurogastroenterol Motil 32(1):e13726

71. Lawson JA, Patrono C, Ciabattoni G, Fitzgerald GA (1986) Long-lived enzymatic metabolites of thromboxane b2 in the human circulation. Anal Biochem 155(1):198–205
72. Kiefer JR, Pawlitz JL, Moreland KT, Stegeman RA, Hood WF, Gierse JK et al (2000) Structural insights into the stereochemistry of the cyclooxygenase reaction. Nature 405(6782):97–101
73. Hammarstrom S (1983) Leukotrienes. Annu Rev Biochem 52:355–377
74. Ohmura T, Tian Y, Sarich N, Ke Y, Meliton A, Shah AS et al (2017) Regulation of lung endothelial permeability and inflammatory responses by prostaglandin a2: role of ep4 receptor. Mol Biol Cell 28(12):1622–1635
75. Zhou W, Zhang J, Goleniewska K, Dulek DE, Toki S, Newcomb DC et al (2016) Prostaglandin i2 suppresses proinflammatory chemokine expression, cd4 t cell activation, and stat6-independent allergic lung inflammation. J Immunol 197(5):1577–1586
76. Ma L, Ni Y, Wang Z, Tu W, Ni L, Zhuge F et al (2020) Spermidine improves gut barrier integrity and gut microbiota function in diet-induced obese mice. Gut Microbes 12(1):1–19
77. Xia T, Duan W, Zhang Z, Li S, Zhao Y, Geng B et al (2021) Polyphenol-rich vinegar extract regulates intestinal microbiota and immunity and prevents alcohol-induced inflammation in mice. Food Res Int 140:110064
78. Sheng K, Yang J, Xu Y, Kong X, Wang J, Wang Y (2022) Alleviation effects of grape seed proanthocyanidin extract on inflammation and oxidative stress in ad-galactose-induced aging mouse model by modulating the gut microbiota. Food Funct 13(3):1348–1359
79. Donati L, Ziegler F, Pongelli G, Signorini MS (1999) Nutritional and clinical efficacy of ornithine alpha-ketoglutarate in severe burn patients. Clin Nutr 18(5):307–311
80. Coudray-Lucas C, Le Bever H, Cynober L, De Bandt JP, Carsin H (2000) Ornithine alpha-ketoglutarate improves wound healing in severe burn patients: a prospective randomized double-blind trial versus isonitrogenous controls. Crit Care Med 28(6):1772–1776
81. Demidenko O, Barardo D, Budovskii V, Finnemore R, Palmer FR, Kennedy BK et al (2021) Rejuvant(r), a potential life-extending compound formulation with alpha-ketoglutarate and vitamins, conferred an average 8 year reduction in biological aging, after an average of 7 months of use, in the truage DNA methylation test. Aging (Albany NY) 13(22):24485–24499
82. Gyanwali B, Lim ZX, Soh J, Lim C, Guan SP, Goh J et al (2022) Alpha-ketoglutarate dietary supplementation to improve health in humans. Trends Endocrinol Metab 33(2):136–146
83. Cynober L, Coudray-Lucas C, de Bandt JP, Guechot J, Aussel C, Salvucci M et al (1990) Action of ornithine alpha-ketoglutarate, ornithine hydrochloride, and calcium alpha-ketoglutarate on plasma amino acid and hormonal patterns in healthy subjects. J Am Coll Nutr 9(1):2–12
84. Filip RS, Pierzynowski SG, Lindegard B, Wernerman J, Haratym-Maj A, Podgurniak M (2007) Alpha-ketoglutarate decreases serum levels of c-terminal cross-linking telopeptide of type I collagen (CTX) in postmenopausal women with osteopenia: six-month study. Int J Vitam Nutr Res 77(2):89–97
85. De Bandt JP, Coudray-Lucas C, Lioret N, Lim SK, Saizy R, Giboudeau J et al (1998) A randomized controlled trial of the influence of the mode of enteral ornithine alpha-ketoglutarate administration in burn patients. J Nutr 128(3):563–569